Petroleum Science 22 (2025) 2274–2289

Contents lists available at ScienceDirect

Petroleum Science

journal homepage: www.keaipublishing.com/en/journals/petroleum-science

Original Paper

Genesis and quantitative evaluation of deep petroleum phase diversity in the Tazhong area, Tarim Basin

Jia-Kai Hou [a], Zhi-Yao Zhang [b, *], Guang-You Zhu [c], Jian-Fa Han [d], Lin-Xian Chi [e], Zi-Guang Zhu [a], Hong-Bin Li [f], Meng-Qi Li [a], Rui-Lin Wang [c]

[a] Research Institute of Petroleum Exploration and Development, PetroChina, Beijing, 100083, China
[b] School of Earth Resources, China University of Geosciences, Wuhan, 430074, Hubei, China
[c] School of Geosciences, Yangtze University, Wuhan, 430100, Hubei, China
[d] Research Institute of Petroleum Exploration and Development, Tarim Oilfield, PetroChina, Korla, 841000, Xinjiang, China
[e] Northwest Oilfield Branch, SINOPEC, Urumqi, 830000, Xinjiang, China
[f] College of Geosciences, China University of Petroleum (Beijing), Beijing, 102249, China

ARTICLE INFO

Article history:
Received 23 June 2024
Received in revised form
28 December 2024
Accepted 17 March 2025
Available online 18 March 2025

Edited by Jie Hao and Meng-Jiao Zhou

Keywords:
Condensate
Gas invasion
Petroleum phase state
GC×GC-TOFMS
Tarim Basin

ABSTRACT

The reservoired petroleum fluids in the deep Ordovician carbonates in the Tazhong area, Tarim Basin, exhibit diverse and intricate geochemical properties and petroleum phases. However, the study on the causal mechanisms for the genesis of co-existed complex petroleum phases and their distribution remains relatively limited. The quantitative assessment of changes in molecular compounds in petroleum pools influenced by secondary alteration to different degrees also needs further investigation. In this study, eight samples including condensate, volatile, and black oil from the Tazhong area were analyzed via GC × GC-TOFMS. The results reveal that condensate oil exhibits complete normal alkane distribution, with abundant diamantanes and organic sulfur compounds (OSCs), and features high density (>0.83 g/cm^3), elevated wax content (>20%), and remarkable gas washing loss. The condensate gas is characterized by highly mature oil-cracking gas with a heavy carbon isotope. Geological analysis indicates that the current Ordovician reservoir temperatures generally remain below 140 °C, which is insufficient to induce in-situ oil cracking. Additionally, black oil pools are formed adjacent to the condensate gas pools, suggesting that the latter is not a result of in-situ oil cracking, but rather represents a secondary condensate gas pool formed through gas invasion of a pre-existed oil pool. Based on the loss of *n*-alkanes and variations in adamantanes (As) and diamantanes (Ds) content across different oil samples, the degree of gas invasion was assessed. We divided gas invasion intensity into strong (Q ≥ 80%, As≥5000 μg/g, Ds ≥ 400 μg/g), weak (20% ≤ Q < 80%, 3000 μg/g ≤ As < 5000 μg/g, 200 μg/g ≤ Ds < 400 μg/g) and negligible (0 ≤ Q < 20%, As < 3000 μg/g, Ds < 200 μg/g). The multistage oil/gas charging events, specifically the sequence of "early oil and late gas" in the Ordovician from the Tazhong area, predominantly drives the phase evolution of reservoired petroleum. Furthermore, differential gas invasion alteration exacerbates the intricacy of petroleum phase distribution. Notably, gas washing processes significantly influence the disparate enrichment of diamondoids homologues in crude oil. Specifically, lower carbon number diamondoids are more abundant in condensate oil, while higher ones exhibit relatively increased abundance in black oil, potentially serving as a valuable quantitative assessment parameter. The findings in this study will provide guiding significance for the analysis and quantitative assessment of deep petroleum phase diversity. Additionally, this research will provide novel insights for comprehensively evaluating basins worldwide with complex petroleum phases distribution.

1. Introduction

From the trending global oil and gas exploration perspective, 92 deep oil and gas pools at depths exceeding 6000 m have been

* Corresponding author.
E-mail address: zhangzhiyao@cug.edu.cn (Z.-Y. Zhang).

https://doi.org/10.1016/j.petsci.2025.03.020

reported and 68 of them have surpassed 8000 m in burial depth (Li et al., 2020a). The exploration and development of deep petroleum resources has become increasingly significant in global oil and gas industry in the future (Dyman et al., 2002). Recent data show that, within the Tarim Basin of China, deep oil and gas accounts for over 90% of the total annually verified geological reserves (Guo et al., 2023), indicating the vast exploration potential in ancient deep oil and gas pools. However, compared to the middle-shallow strata, deep strata generally have experienced multiple periods of charging (Li et al., 2020a), possess complex dynamic mechanism and hydrocarbon accumulation distribution (Zhu et al., 2023). Therefore, deep oil and gas geochemical properties and phases have obvious particularity and complexity.

The Tarim Basin, located in western China, represents the largest and most prolific petroliferous basin with the most complex geological conditions (Wang et al., 2024a) (Fig. 1(a)). Within this basin, the Ordovician carbonate reservoirs of Tazhong Uplift is the primary zone with increasing hydrocarbon production (Zhu et al., 2018), boasting immense resource potential. The controversy over the source of deep petroleum in the Tazhong area has lasted for more than twenty years. Previous research has shown that most crude oils in the Tarim Basin are characterized by a low abundance of dinoflagellate steranes, 4-methyl steranes, 24-norcholestanes, 24-nor rearranged steranes, gammaceranes, C_{28} regular steranes, and a high abundance of rearranged steranes (Li et al., 2010, 2021; Lu et al., 2024). The Middle-Upper Ordovician source rocks have similar biomarker characteristics to those of marine crude oils. However, the distribution range of Ordovician source rocks is limited, and the thickness and abundance of organic matter are small, so they are not sufficient to be the main source rocks (Zhu et al., 2018). Recently, with the discovery of high-quality source rocks from the Lower Cambrian Yurtus Formation in outcrops in the Tarim basin, more and more evidence, including drilling core, light hydrocarbon fingerprint chromatography, and sulfur isotopes of crude oils, supports that the Lower Cambrian Yurtus Formation is the main hydrocarbon source rock in the Tarim Basin (Luo et al., 2024; Zhang et al., 2024a).

In recent years, tremendous oil and gas exploration efforts have revealed notable regional variations in the phase types. Previous research suggests that hydrocarbon composition, temperature, and pressure systems are key factors influencing the diversity of petroleum phases (Danesh, 1998). However, the influencing factors on the phase types of deep Ordovician petroleum in the Tazhong area may be more intricate. The Tarim Basin has undergone prolonged burial and has experienced multiple episodes of overlapping and tectonic adjustments (Bian et al., 2023), resulting in the coexistence of different phase types including heavy oil, light oil, volatile oil, condensate, and natural gas within the same zone (Zhang et al., 2022). The diversity of deep petroleum phase may be attributed to multiple episodes of hydrocarbon charging events and post-accumulation secondary alterations (Zhu et al., 2019). Within the Ordovician carbonate pools of the Tazhong Uplift, three phases of fluid inclusions have been identified (Han et al., 2012): two oil phases (Late Caledonian and Late Hercynian) and one gas phase (Himalayan), indicating three distinct episodes of hydrocarbon charging and reservoir formation in the Tazhong area (Zhang et al., 2010). The tectonic activity weakened after the Hercynian period, greatly favoring the preservation of oil and gas pools. However, during the Himalayan period, localized adjustments in the fault system of the Tazhong Uplift resulted in fracture intersection points often serving as initiation sites for gas invasion (Pang et al., 2013). The gas, derived from the over-mature Cambrian source rocks and the cracked paleo oil pools, migrated upward along faults to undergo varying degrees of gas invasion into the Ordovician pre-exist oil pools, leading to characteristics of condensate gas in the outer zones and crude oil in the inner zones (Han et al., 2007). This process further induced anomalous distributions and systematic lateral variations in the chemical composition and physical properties of crude oil (Zhang et al., 2018b).

Methods for identifying complex petroleum phases primarily include high-temperature high-pressure fluid experiments (PVT) conducted on reservoired fluids (Maxwell, 2011), as well as empirical discrimination methods based on the physical properties and fluid components (Kontogeorgis and Ioannis, 2010). However, gas invasion induces differentiation in the physical and chemical properties of oil and gas (Zhu et al., 2021), leading to changes in phase. Thompson simulated gas invasion fractionation effects by repeatedly injecting methane into normal crude oil in a series of experiments (Thompson, 1983), proposing the evaporative fractionation theory to explain the formation mechanism of non-thermogenic condensates. Various degrees of gas invasion fractionation can result in changes in fluid composition and properties within oil and gas pools (Han et al., 2021), with fluid property evaluation parameters typically exhibiting a strong linear relationship with gas invasion intensity (Zhu et al., 2014), offering significant discrimination capability for the gas invasion intensity. As a consequence of gas invasion, various components are redistributed between gas and liquid phases. Based on the wax content (*n*-heptane/methylcyclohexane) and aromaticity (toluene/*n*-heptane), it proposed that crude oil samples from the Alaska North Slope had experienced varying degrees of gas invasion (Masterson et al., 2001). Carbon isotopes of natural gas can similarly discern the intrusion of allochthonous gas sources into oil and gas pools, incorporating highly mature dry gas resulting in heavy carbon isotopes of methane (Zhu et al., 2021). However, current evaluations of the deep petroleum phase in the Tazhong Uplift are largely confined to qualitative assessments, lacking systematic and detailed quantitative evaluations of the molecular compositions of multiphase pools under different intensities of secondary alteration. Furthermore, there is a dearth of organic integration between gas invasion intensity and variations in the content of diamondoids. Additionally, the distribution characteristics and dynamic evolution processes of complex petroleum phases in deep strata remain relatively unclear.

This study focuses on the complex distribution characteristics of complex petroleum phases in deep strata in the Ordovician strata of the Tazhong Uplift, Tarim Basin, aiming to provide insights into the causal mechanisms and quantitative analysis of deep petroleum phase diversity from a molecular geochemical perspective. Leveraging the advantages of techniques such as comprehensive two-dimensional gas chromatography coupled to time-of-flight mass spectrometry (GC × GC-TOFMS) with ultra-high resolution and sensitivity, large peak capacity, accurate qualitative and quantitative results, and compound groups separation characteristics (Wang et al., 2012), we achieved detailed interpretation of molecular compound series with extremely low contents in oil samples, including diamondoids, thiadiamondoids, and ethanodiamondoids. By dissecting these low-content molecular compound series, we aim to unveil the mechanisms of petroleum phase transformation, which can guide predictions of the spatial distribution of petroleum phase in deep strata, providing theoretical support for the exploration and development of special complex oil and gas resources in deep to ultra-deep area.

2. Geological settings

The Tarim Basin, covering an area of approximately 56×10^4 km^2, is surrounded by the Tianshan, Kunlun, and Altun mountains. It is a superimposed basin formed by the combination of Mesozoic and Cenozoic continental foreland basins and

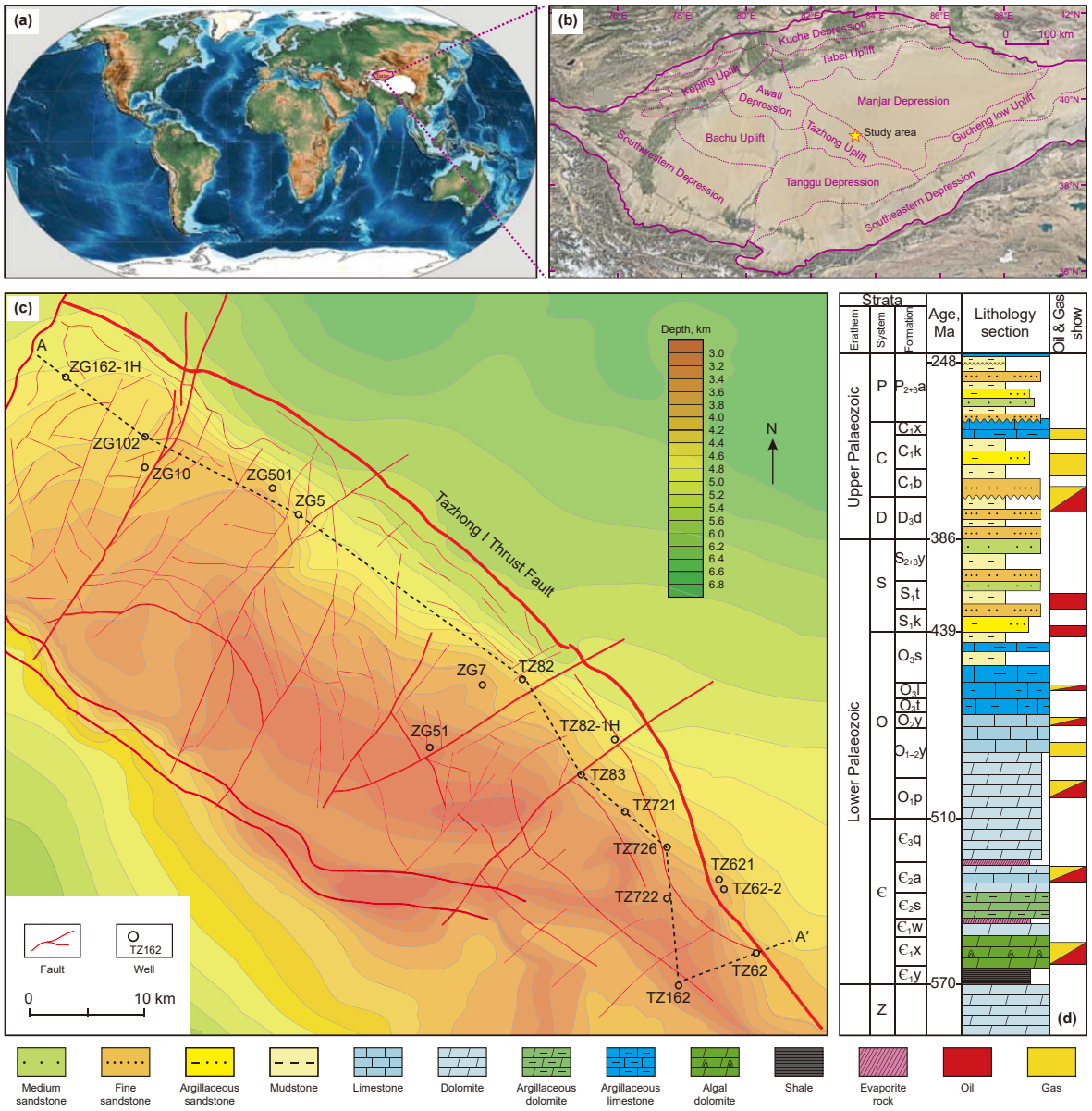

Fig. 1. Location of the Tarim Basin in China in the global plate map **(a)**, regional tectonic division and location of study area in Tarim Basin **(b)**, structural map **(c)**, and general stratigraphic column **(d)** of the Tazhong Uplift, Tarim Basin. Notes: $P_{2+3}a$, the Middle-upper Permian Akekule Formation; C_1x, the Lower Carboniferous Xiaohaizi Formation; C_1k, the Lower Carboniferous Kalashayi Formation; C_1b, the Lower Carboniferous Bachu Formation; D_3d, the Upper Devonian Keziertage Formation; $S_{2+3}y$, the Middle-Upper Silurian Yimugantawu Formation; S_1t, the Lower Silurian Tataaiertage Formation; S_1k, the Lower Silurian Kepingtage Formation; O_3s, the Upper Ordovician Sangtamu Formation; O_3l, the Upper Ordovician Lianglitage Formation; O_3t, the Upper Ordovician Tumuxiuke Formation; O_2y, the Middle Ordovician Yijianfang Formation; $O_{1\text{-}2}y$, the Lower-Middle Ordovician Yingshan Formation; O_1p, the Lower Ordovician Penglaiba Formation; ϵ_3q, the Upper Cambrian Qiulitage Formation; ϵ_2a, the Middle Cambrian Awatage Formation; ϵ_2s, the Middle Cambrian Shayilike Formation; ϵ_1w, the Lower Cambrian Wusonggeer Formation; ϵ_1x, the Lower Cambrian Xiaoerbulake Formation; ϵ_1y, the Lower Cambrian Yuertusi Formation; Z, Sinian (Precambrian).

Paleozoic marine craton basins (Zhang et al., 2022, 2024b). Undergoing multiple episodes of subsidence and uplift, it has developed the present structural pattern of "four uplifts and five depressions" (Jin and Cai, 2007). The main structural units include the Bachu, Tazhong, Tabei, and Tadong Uplifts, as well as the Tanggu, Southeast, Northern, Southwest, and Kuche Depressions (Fig. 1(b)). The Tazhong Uplift is located in the central part of the Tarim Basin. The northeast is bounded by Tazhong 1 fault and adjacent to the Manjar depression. It is adjacent to the Tanggu depression in the south in the form of thrust fault, and adjacent to Bachu Uplift in the west, delineated by the Tumuxiuke Fault, forming a nose-shaped uplift sloping from northeast to southwest (Fig. 1(c)). In this study, the eastern part of the Tazhong area (east of well ZG162-1H and west of well TZ62) was selected as the research area, with "Tazhong" referring only to this specific region in the text.

The Tazhong Uplift is an inherited anticline formed in the Cambrian-Ordovician carbonate rocks based on a Paleozoic uplift (Zhang et al., 2012). Influenced by north-south compressional stress, the Tazhong 1 fault zone underwent strong north-eastward thrusting, resulting in the north-eastward structural pattern of the Tazhong Uplift (Lv et al., 2009). By the end of the Ordovician (Late Silurian), the structural pattern of the Middle Ordovician was inherited in the Tazhong area, with the paleo-uplift being basically established. At the end of the Silurian, erosion occurred under the influence of southwest-directed tectonic activity, forming north-

eastward strike-slip faults (Fig. 1(c)). During the Carboniferous, overall subsidence began, resulting in extensive and stable intracraton deposition, with localized compressional effects, but the morphology and distribution of the Cambrian-Ordovician uplift anticlines remained largely unchanged (Li et al., 2009), displaying inheritance development. The stratigraphy in the Tazhong area is well-developed, primarily comprising the Lower Paleozoic Cambrian, Ordovician, and Silurian, as well as the Upper Paleozoic Devonian, Carboniferous, and Permian. In most areas, the Sinian strata are conspicuously absent (Zhang et al., 2024b). The complete Ordovician strata in the Tazhong area consist specifically of the Lower Penglaiba Formation (O_1p) and Yingshan Formation ($O_{1\text{-}2}y$), the Middle Yijianfang Formation (O_2y), the Upper Tumuxiuke Formation (O_3t), Lianglitage Formation (O_3l), and Sangtamu Formation (O_3s) (Fig. 1(d)). The Cambrian strata include the Lower Yuertusi Formation (ϵ_1y), Xiaoerbulake Formation (ϵ_1x), and Wusonggeer Formation (ϵ_1w), the Middle Shayilike Formation (ϵ_2s) and Awatage Formation (ϵ_2a), and the Upper Qiulitage Formation (ϵ_3q).

The Tarim Basin exhibits a low geothermal gradient (2 °C/100 m), with a lagged compensatory effect between time and temperature (Zhu et al., 2023). The hydrocarbon accumulation in deep reservoirs is controlled by various factors such as temperature, pressure, reserving space, and fluid activity, displaying characteristics of multistage composite accumulation (Jia and Zhang, 2023). Due to the huge burial depth, the Tazhong area lacks effective hydrocarbon source rock samples for oil and gas source correlation. Previous studies suggested that hydrocarbon supply includes Cambrian-Lower Ordovician and Middle-Upper Ordovician marine source rocks, which contribute variously in different structural positions (Huang et al., 2016; Zhang et al., 2012). However, recent research indicates that the main source rocks of the Ordovician are more related to the black shale of the Lower Cambrian Yuertusi Formation, determining the favorable geological conditions for deep oil and gas exploration in the Tarim Basin (Zhang et al., 2022).

The Ordovician strata in the Tazhong area are primarily characterized by the development of reef-bank reservoirs in the Lianglitage Formation and karst-fracture reservoirs in the Yingshan Formation. Within the Lianglitage Formation, reef-bank reservoirs are mainly developed in two high-energy sedimentary facies: the platform margin reef and inner platform shoal. These reservoirs often undergo multiple dissolution and alteration processes, resulting in the formation of large-scale fracture-cavity complexes, thereby constituting a cavity-reef-bank reservoir system (Han et al., 2007). They are predominantly distributed in the Tazhong 1 fault zone at the northern margin of the Bachu-Tazhong Platform (Yang et al., 2011). The karst-fracture reservoirs in the Yingshan Formation experienced rapid subsidence and continuous burial after late-stage hydrocarbon charging, thereby preserving the spatial structure and storage capacity developed during the early stages (Zhang et al., 2018a). Two types of high-quality reservoirs exist, in conjunction with the widespread occurrence of mudstone and argillaceous limestone caprock in the Sangtamu Formation and mudstone caprock in the Tumuxiuke Formation. These elements form a favorable reservoir-seal assemblage and represent the primary hydrocarbon-bearing strata of the Ordovician in the Tazhong area.

3. Materials and methods

The molecular composition of eight different types of Ordovician oil samples in the Tazhong area, including condensate oil (TZ62, ZG102, TZ82, TZ83), volatile oil (ZG5 and TZ726), and heavy oil (TZ162 and ZG162-1H), were analyzed using GC × GC-TOFMS. The GC × GC-TOFMS analysis utilized a DB-Petro column (50 m × 0.2 mm × 0.5 μm) as the first dimension (1D) column, with a temperature program starting at 35 °C for 0.2 min, followed by an increase at a rate of 1.5 °C/min to 210 °C for 0.2 min, and further increased at a rate of 2 °C/min to 300 °C, with a hold time of 20 min. The second dimension (2D) column was a DB-17HT column (3 m × 0.1 mm × 0.1 μm), using the same temperature program as the 1D column with a 5 °C higher temperature. The solvent used was CH_2Cl_2, and D16-adamantane was added to the oil samples as an internal standard. The composition of molecular compounds in the oil samples was quantitatively determined using the peak area normalization method.

The associated gases from the reservoirs were analyzed for alkane gas composition using an Agilent 7890 gas chromatograph, GC oven temperature was initially set at 70 °C for 5 min, and then ramped to 180 °C at 15 °C/min, and finally maintained at 180 °C for 15 min. All the gas compositions were corrected for oxygen and nitrogen (Dai et al., 2016).

A Thermo Delta V Advantage instrument was used for the stable carbon isotopic measurements of the gas samples, individual hydrocarbon gas components (C_1–C_4) and CO_2 were separated on a gas chromatograph using a fused silica capillary column (PLOT Q 27.5 m × 0.32 mm × 10 μm) followed by conversion into CO_2 in a combustion interface, and then injected into the mass spectrometer (Dai et al., 2016).

4. Results

4.1. Phase type and distribution of deep petroleum

The spatial distribution of the petroleum phase of Ordovician in the Tazhong area is complex (Zhu et al., 2014). Various petroleum phases, including saturated and unsaturated condensate, volatile oil, and black oil, were identified using the fluid PVT phase diagram method, reservoir fluid ternary discrimination method (The component contents of C_1+N_2, C_2-C_6+CO_2 and C_{7+}), and box plot method (Four component parameters: $100C_2/C_1$, $100C_2/(C_3+C_4)$, C_2/C_3 and C_{2+}).

A northwest-southeast cross-section illustrates the complex spatial distribution of petroleum phase in the Tazhong area (Fig. 2). Overall, the distribution of petroleum phase is significantly influenced by strike-slip faults and structural amplitudes. Major strike-slip faults penetrate the basement, connecting to deep Cambrian source rocks. Oil and gas are mainly distributed along these major faults or their associated secondary faults, with no unified oil-water contact. Condensate gas pools, primarily saturated or unsaturated, are mainly developed near the Tazhong 1 fault and northeast-trending strike-slip faults, as well as local structural highs, such as the wells ZG102, TZ82, TZ83, TZ721, and TZ62, exhibiting high gas-oil ratios and high productivity. Oil pools are mainly developed in block interiors or at higher positions far from faults, such as the wells ZG162-1H, TZ722, and TZ162, with relatively lower gas-oil ratios and productivity. Some areas, such as the wells ZG5 and TZ726 near faults, but phase analysis indicates that volatile oil pools close to the critical state of condensate pools.

4.2. Physical properties of oil and gas

The physical properties of condensate oil and black oil in the study area exhibit significant differences (Table 1). The density of condensate oil ranges from 0.778 to 0.833 g/cm^3 (measured at 20 °C), with an average of 0.814 g/cm^3. The relative content of wax, resin + asphaltenes, and sulfur is in the range of 3.5%–22.5% (average of 12.6%), 0.22%–0.40% (average of 0.32%), and 0.08%–0.38% (average of 0.24%), respectively. On the other hand, the mean density of black oil is 0.799 g/cm^3 (measured at 20 °C). It is unusual

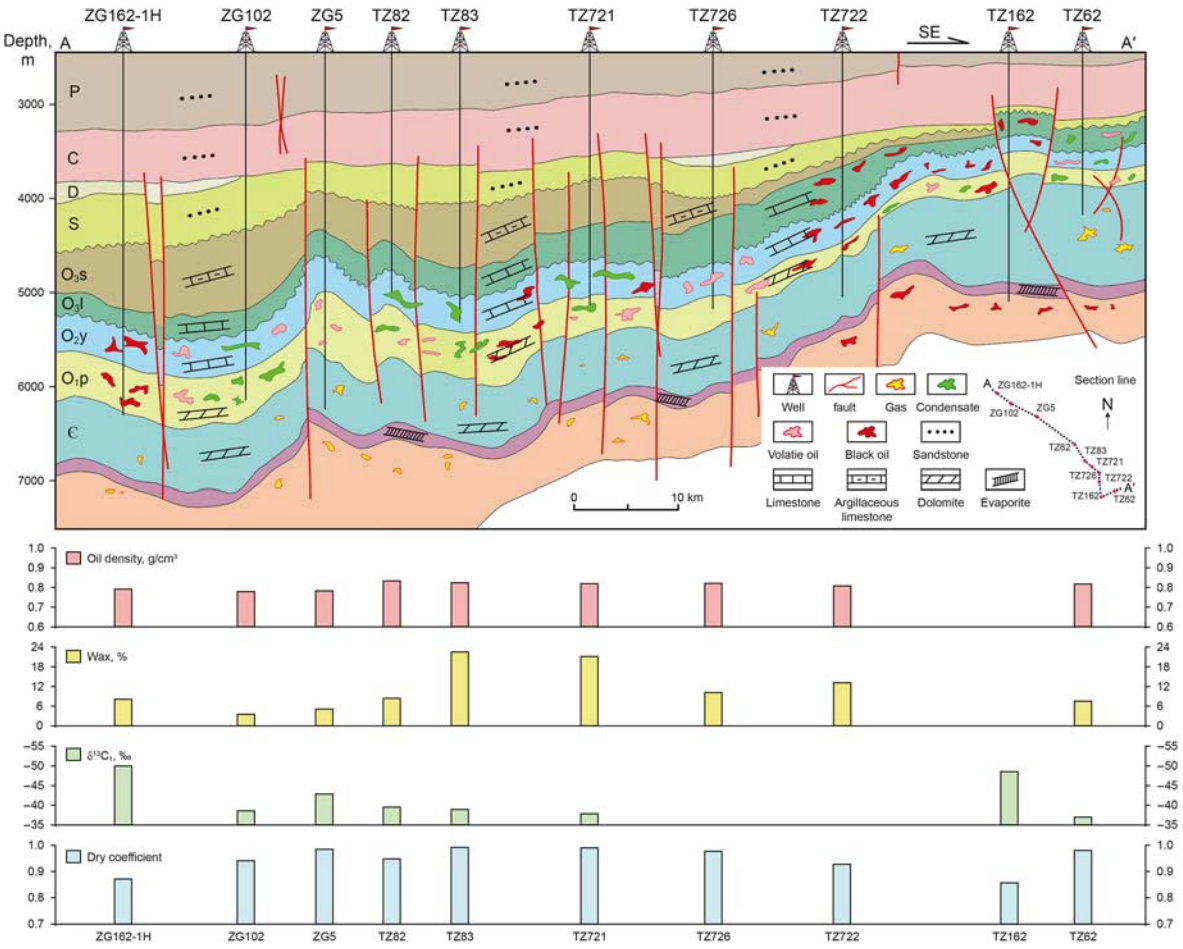

Fig. 2. A NW-SE geological cross section, petroleum phase distribution, oil densities (20 °C), wax, gas dryness and $\delta^{13}C$ of oil-dissolved methane in the Tazhong area.

that condensate oil is heavier than black oil.

The hydrocarbon gas components account for 87.32%–96.59% in the natural gas chemical composition. Non-hydrocarbon gases are mainly composed of N_2 (0.65%–7.12%) and CO_2 (0.65%–8.24%), with some samples containing higher levels of H_2S. The carbon isotope ratios in natural gas increase with the relative molecular weight, showing a positive carbon isotope profile of $\delta^{13}C_1 < \delta^{13}C_2 < \delta^{13}C_3 < \delta^{13}C_4$ (Table 2). The condensate gas is generally dry, with a maximum dryness coefficient of 0.991, and its methane carbon isotope composition is relatively heavy, indicating a higher thermal maturity. Conversely, the black oil-associated gas is predominantly wet gas, with dryness coefficients ranging from 0.856 to 0.927, and its methane carbon isotope composition is relatively light. Therefore, the Ordovician condensate pools commonly exhibit the characteristic of "dry gas and heavy oil".

Table 1
Physical properties and light hydrocarbon composition parameters of crude oil.

Well	Type	Depth, m	Density, g/cm³		Viscosity, mPa·s	Wax, %	Resin, %	Asphaltene, %	Resin + asphaltene, %	Sulfur, %	Water, %	nC_7/MCH	Tol/nC_7
			20 °C	50 °C									
TZ62	Condensate	4758	0.817	0.800	2.03	7.5	0.22	0.13	0.35	0.08	12.23	2.37	0.35
TZ82	Condensate	5385	0.833	0.810	3.43	8.4	0.39	0.01	0.40	0.24	/	2.31	0.37
TZ83	Condensate	5681	0.823	0.800	3.18	22.5	/	/	/	0.38	16.65	2.51	0.48
TZ721	Condensate	5505	0.819	0.800	2.65	21.2	/	/	/	0.27	1.02	2.44	0.56
ZG102	Condensate	6060	0.778	0.756	1.21	3.5	0.10	0.12	0.22	0.21	/	2.30	0.26
TZ726	Volatile oil	5535	0.821	0.800	2.28	10.1	0.51	0.09	0.60	0.18	4.77	3.00	0.10
ZG5	Volatile oil	6460	0.782	0.759	1.22	5.1	0.66	0.26	0.92	/	/	2.75	0.17
TZ722	Black oil	5750	0.807	0.780	1.91	13.1	1.15	0.30	1.45	0.08	1.94	3.88	0.13
TZ162	Black oil	5070	/	/	/	/	/	/	/	/	/	3.47	0.04
ZG162-1H	Black oil	6175	0.791	0.769	1.84	8.1	0.81	0.05	0.86	0.15	/	3.15	0.07

Note: MCH: Methylyclohexane; Tol: Toluene.

Table 2
Gas composition and carbon isotopes in the study area.

Well	Depth, m	Gas component, %								Dryness coefficient	Carbon isotopic values, ‰			
		C_1	C_2	C_3	iC_4	nC_4	N_2	CO_2	H_2S, mg/m^3		$\delta^{13}C_1$	$\delta^{13}C_2$	$\delta^{13}C_3$	$\delta^{13}C_4$
TZ62	4758	90.70	1.37	0.30	0.09	0.14	4.17	3.05	2600	0.980	−37.0	−31.5	−29.9	/
TZ82	5385	86.30	3.75	0.36	0.22	0.40	7.12	1.03	/	0.948	−39.5	−33.7	−30.5	−29.0
TZ83	5681	93.10	0.64	0.10	0.04	0.06	0.97	4.91	32000	0.991	−38.9	−32.2	−28.0	−26.7
TZ721	5505	92.10	0.65	0.14	0.04	0.07	2.08	4.33	100	0.990	−37.8	−35.6	−31.6	−29.8
ZG102	6060	87.63	2.24	1.42	0.74	1.07	3.73	2.17	22100	0.941	−38.5	−31.4	−29.2	−29.0
TZ726	5535	92.30	1.76	0.22	0.08	0.07	0.90	4.56	/	0.977	−40.5	−30.8	−23.4	/
ZG5	6460	90.90	1.06	0.25	0.09	0.09	0.65	5.39	19000	0.984	−42.8	−32.5	−29.5	−28.7
TZ722	5750	81.40	3.18	1.58	0.58	1.06	2.50	8.24	/	0.927	/	/	/	/
TZ162	5070	82.70	7.73	3.99	0.53	1.64	1.58	0.65	/	0.856	−48.5	−40.2	−35.5	−32.9
ZG162-1H	6175	71.95	6.08	4.52	1.69	3.08	4.23	3.10	/	0.872	−49.9	−36.3	−31.3	−30.9

4.3. Bulk composition

GC × GC-TOFMS analysis was conducted on eight oil samples from the study area. The samples were directly injected to minimize the loss of light components and to separate the molecular compounds within the oil samples effectively. Each individual compound appeared as a distinct circular area in the 2D chromatogram and as separate peaks in the 3D contour plot (Fig. 3). The peak area and peak height in the chromatogram reflected the abundance of each compound. Three representative oil samples, ZG102, TZ726, and TZ162, were selected to compare the condensate oil, volatile oil, and heavy oil within the study area. Compounds with a signal-to-noise ratio greater than 100 were structurally identified, revealing certain differences in the compound groups among different types of oil samples. The compound compositions covered a range from C_6 to C_{30} (Fig. 3).

The GC × GC exhibited the capability of separating compound groups and the "tile effect" is obvious. The major compound groups include aliphatic (*n*-alkanes and cycloalkanes), aromatic (benzenes, naphthalenes and phenathrenes, etc), diamondoids (adamantanes, diamantanes and triamantanes), ethanodiamondoids, and sulfur compounds (thiadiamondoids, tetrahydrothiophenes, benzothiophenes and dibenzothiophenes). It can be observed that the distribution of diamondoids and sulfur

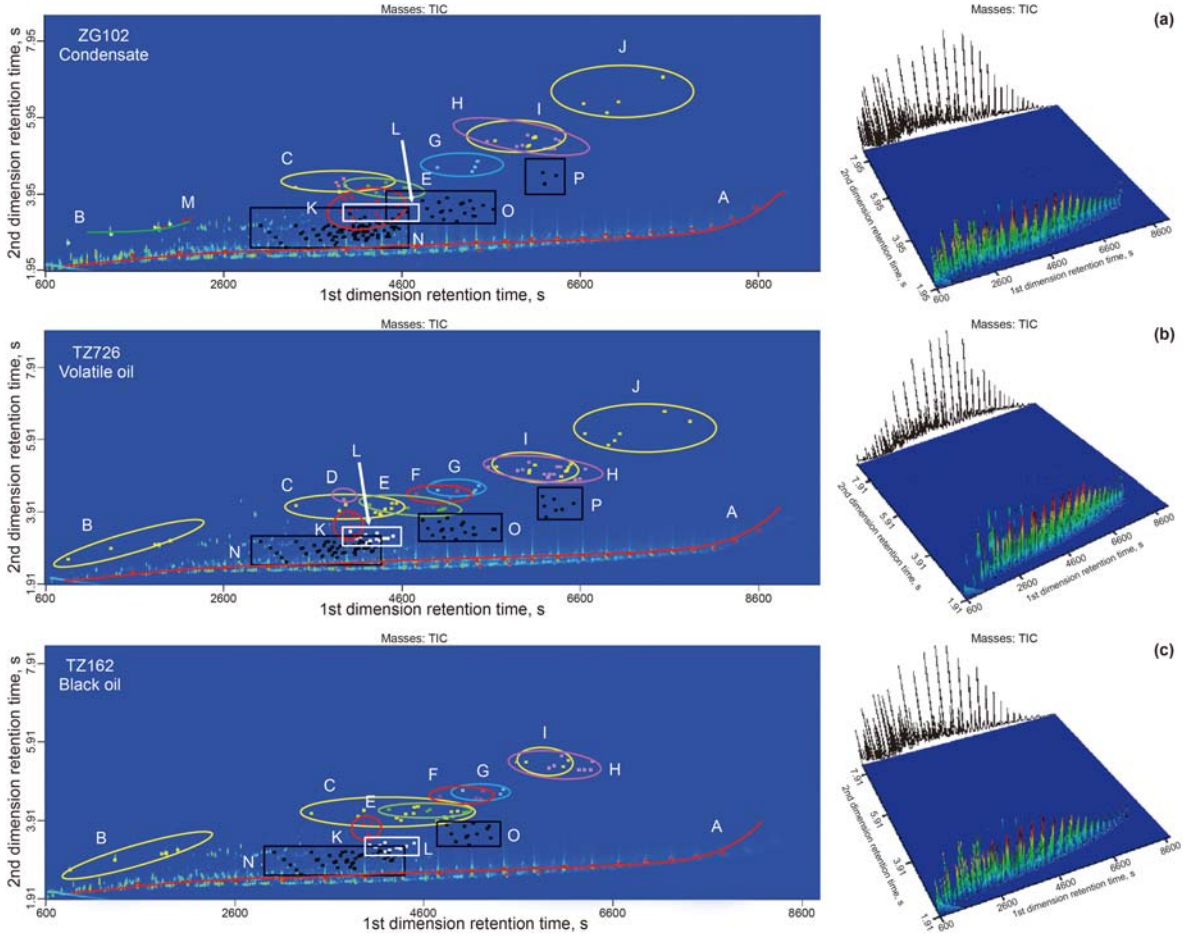

Fig. 3. GC × GC-TOFMS color contour chromatograms and the corresponding 3D plot of the condensate oil, volatile oil and black oil sample in the study area. Notes: A, alkanes; B, benzenes; C, naphthalenes; D, benzothiophenes; E, biphenyls; F, dibenzofurans; G, fluorenes; H, dibenzothiophenes; I, phenathrenes; J, pyrenes; K, thiaadamantanes; L, ethanodiamondoids; M, tetrahydrothiophenes; N, adamantanes; O, diamantanes; P, triamantanes.

compounds varies significantly, with higher enrichments in volatile oil and condensate oil.

4.4. Distribution of diamondoids

Diamondoids are a type of cycloalkanes consisting solely of C and H elements, connected by single bonds within the molecule. They exhibit higher thermal stability and greater resistance to cracking compared to saturated hydrocarbons with same carbon number (Wei et al., 2006). The comprehensive two-dimensional chromatogram under specific selected ions demonstrated excellent separation of diamondoids (Fig. 4), identifying diamondoids with one to three cages from the Tazhong samples. In the 2D contour plot, peaks corresponding to the same carbon number of diamondoids isomers appeared as straight lines, while "tile effect" was observed for diamondoids between different carbon numbers.

The content of diamondoids decreased with increasing the number of cages, and compared to adamantanes, each oil sample exhibited fewer amounts of diamantanes and triamantanes. A total of 64, 50, and 36 adamantanes were detected in the condensate oil, volatile oil, and heavy oil, respectively. Combining with previous studies on the structure of diamondoids (Azevedo et al., 2008; Dahl et al., 2002; Wei et al., 2006), 19 alkyl adamantanes with confirmed structures were detected, with total contents of 5656.2, 4608.7, and 1096.6 μg/g in the condensate oil, volatile oil, and heavy oil, respectively. The total contents of confirmed diamantanes were 524.3, 398.4, and 172.8 μg/g, respectively.

4.5. Distribution of organosulfur compounds

Differences in the types and abundance of sulfur compounds were observed among different oil samples, with the highest diversity and concentration found in the condensate oil sample, primarily comprising tetrahydrothiophenes (m/z = 101), thiaadamantanes (m/z = 153, 177, 191), alkyl benzothiophenes (m/z = 147, 161, 175), and alkyl dibenzothiophenes (m/z = 184, 198, 212). In contrast, only a small amount of thiaadamantanes and dibenzothiophenes were detected in the heavy oil sample (Fig. 5). Thiaadamantanes are indicative products of thermochemical sulfate reduction (TSR) between hydrocarbons and sulfates (Amrani, 2014), and their concentration levels reflect the intensity of TSR (Gvirtzman et al., 2015). Fourteen species of thiaadamantanes were detected in the sample ZG102, with seven structurally confirmed species, totaling 58.9 μg/g. Seven species of thiaadamantanes were found in the sample TZ726, totaling 16.5 μg/g, while only three species were detected in the sample TZ162, totaling 7.5 μg/g. Overall, there is a gradual decrease in both the types and abundance of sulfur compounds from condensate oil to volatile oil and then to black oil.

5. Discussion

5.1. Gas invasion and formation of petroleum phase diversity

5.1.1. Oil and gas composition and physical property variations

According to conventional petroleum geology theory, oil density

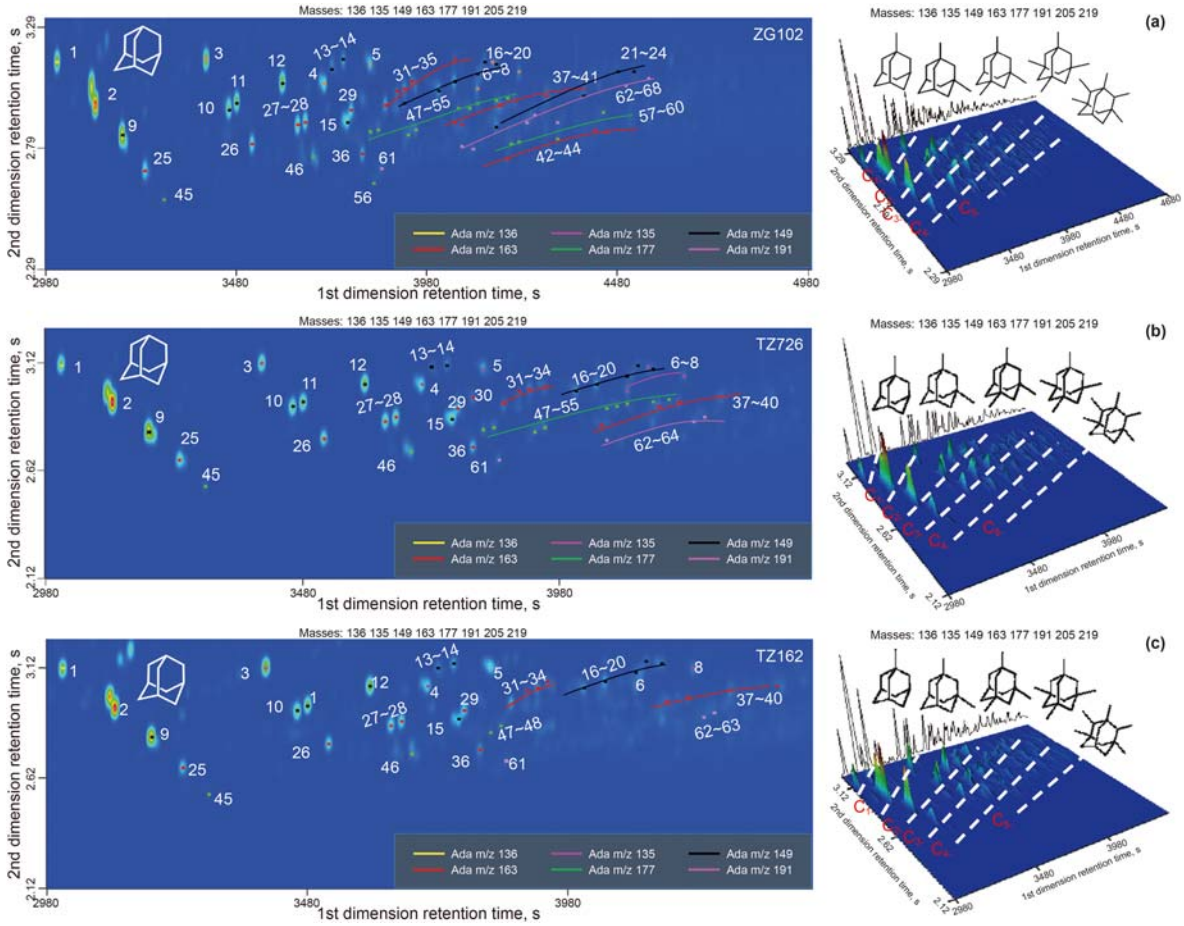

Fig. 4. Adamantane compounds detected using extracted ion chromatogram (m/z 135, 136, 149, 163, 177, 191, 205 and 219) and the corresponding 3D plot of the ZG102 **(a)**, TZ726 **(b)** and TZ162 **(c)** oil sample from the Tazhong area, Tarim Basin.

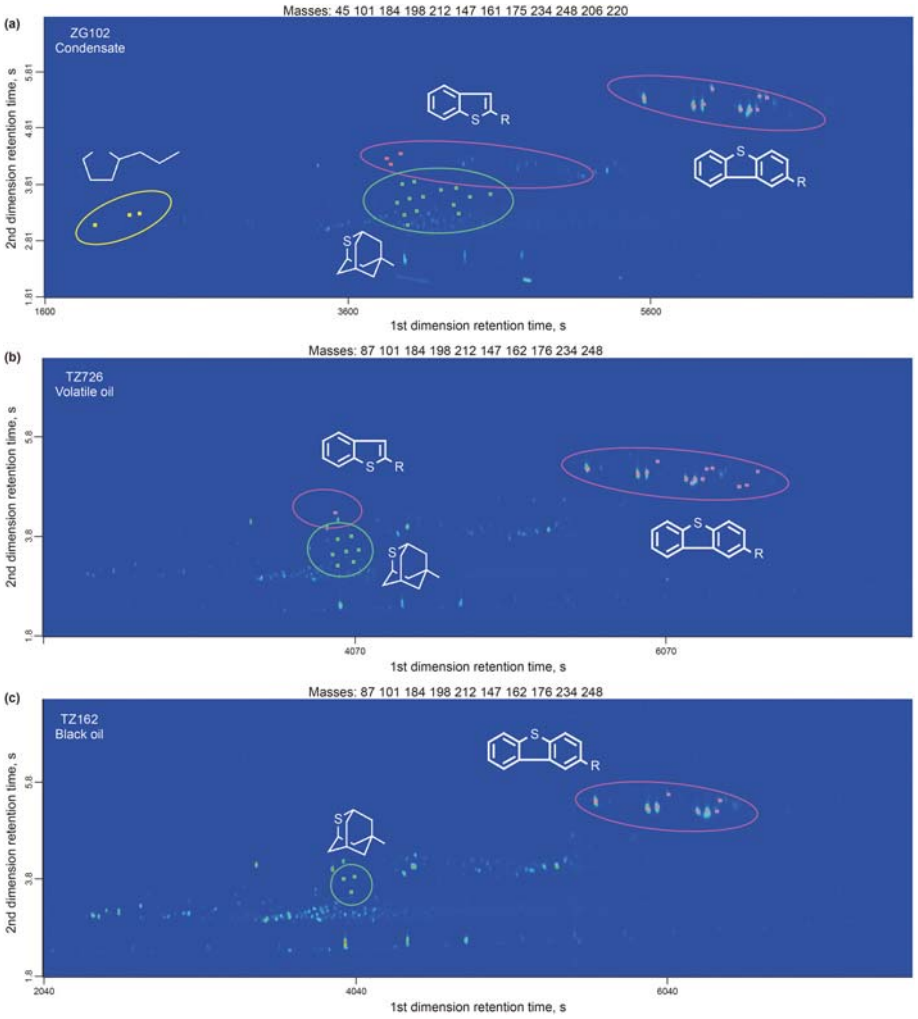

Fig. 5. **(a)** GC × GC-TOFMS color contour chromatogram for *m*/*z* 45, 101, 184, 198, 212, 147, 161, 175, 234, 248, 206, 220 of sulfur-containing compounds in the condensate of well ZG102; **(b)** *m*/*z* 87, 101, 184, 198, 212, 147, 162, 176, 234, 248 of sulfur-containing compounds in the volatile oil of well TZ726; **(c)** *m*/*z* 87, 101, 184, 198, 212, 147, 162, 176, 234, 248 of sulfur-containing compounds in the black oil of well TZ162.

generally decreases with increasing thermal maturation degree during oil and gas generation stage. Typically, in higher maturation stage (R_o > 1.3%), the primary thermogenic condensate oil generated usually has a density around 0.7 g/cm^3, with the condensate gas predominantly wet (Li et al., 2020b). In contrast, the characteristics of the Tazhong condensate oil and gas are markedly contradictory to the expected (Tables 1 and 2), characterized by heavier oil with high wax content and extremely dry gas (dryness coefficient approaching 1), distinctly different from the black oil-associated gas. Although the associated gas with volatile oil has slightly lower dryness coefficients, it also falls within or close to the range of dry gas, and only the associated gas with black oil being relatively wet, with ethane content exceeding 3%.

The oil and gas resources in the Tazhong area are mainly sourced from the Lower Cambrian source rocks (Zhu et al., 2018), potentially generating significant amounts of oil during the Late Caledonian to Late Hercynian periods, while natural gas generation occurred during the Late Himalayan burial processes (Han et al., 2021). Therefore, the Tazhong area has undergone multiple episodes of hydrocarbon migration and charging, complex hydrocarbon accumulation, and late-stage alteration (Zhang et al., 2015). Paraffinicity (*n*-C_7/MCH) and aromaticity (Tol/*n*-C_7) are two common parameters used to interpret secondary alterations such as gas invasion, which may change the relative concentrations of some light hydrocarbons, resulting in a decrease in parafnicity and an increase in aromaticity at the same time. The cross-plot of light hydrocarbon parameters (Fig. 6) shows that black oils have the lowest aromaticity and relatively high paraffinicity while condensates have significantly higher aromaticity and lower paraffinicity. Observed gradual changes in light hydrocarbon components in oils with different phases indicate the occurrence of gas invasion, and the fractionation from black oil to condensate shows a gradual enhancement.

The higher density of condensate oil is due to the enrichment of wax (up to 20%), which is unlikely to be caused by the thermal evolution of source rocks or crude oil. A more plausible explanation is that the volume expansion of crude oil caused by gas invasion causes some gas-filled light crude oil to overflow the pool and migrate upward along the fault as liquid phase. During the process of crude oil migration, due to the gradual decrease in formation temperature and pressure, petroleum components continue to differentiate, and liquid components with larger molecular weights gradually precipitate to form waxy crude oil. In other words, the condensate samples in Tazhong area analyzed in this study are likely to be mainly gas invasion fractionation residues. Consequently, the condensate oil has high wax content and density, with the natural gas being dry.

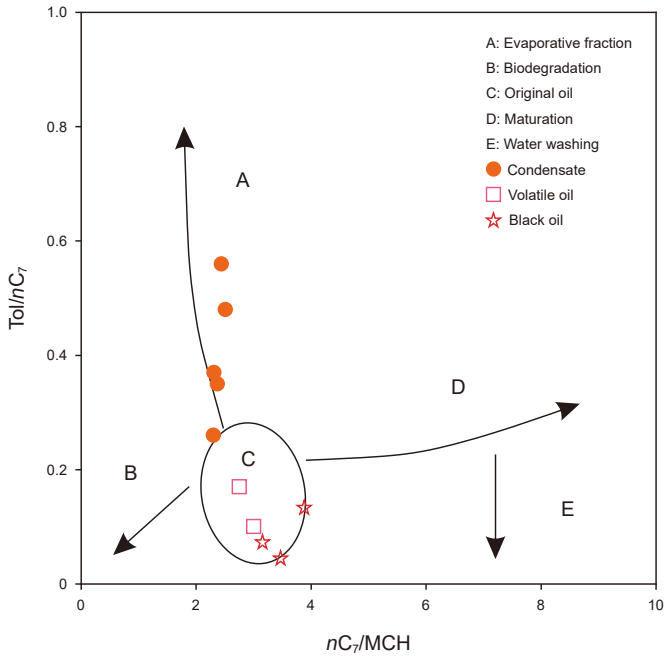

Fig. 6. Light hydrocarbon parameters in different types of crude oil (modified after Thompson, 1987). Tol = Toluene, nC_7 = *n*-Heptane, MCH = Methylcyclohexane.

5.1.2. Oil and gas maturity difference

5.1.2.1. Oil maturity parameters. Due to the differential thermal stability among compounds of the same class with varying substituents and minimal influence of biodegradation, aromatic hydrocarbon compounds present in crude oil serve as suitable indicators. Thus, they are suitable for identifying products at mature and highly mature thermal evolution stages (Zhang and Huang, 2005). The methyl phenanthrene index (MPI) of phenanthrene series compounds within the aromatic hydrocarbon fraction was employed for crude oil maturity assessment (Radke, 1983):

$$MPI_1 = 1.5 \times (3\text{-MP} + 2\text{-MP})/(P + 9\text{-MP} + 1\text{-MP}) \quad (1)$$

$$MPI_2 = 3 \times 2\text{-MP}/(P + 9\text{-MP} + 1\text{-MP}) \quad (2)$$

In Eqs. (1) and (2), P = phenanthrene; 1-MP = 1-methylphenanthrene; 2-MP = 2-methylphenanthrene; 3-MP = 3-methylphenanthrene; 9-MP = 9-methylphenanthrene.

The relationship between MPI and Rc (equivalent vitrinite reflectance) is (Zhang and Huang, 2005):

$$Rc_1 = 0.6 \times MPI_1 + 0.4 \ (R_o < 1.3\%) \quad (3)$$

$$Rc_1 = -0.6 \times MPI_2 + 2.3 \ (R_o > 1.3\%) \quad (4)$$

According to the distribution range of MPI_1 and MPI_2, the calculated Rc_1 is between 1.00% and 1.86%, which belongs to mature-high mature crude oil (Table 3).

In high-over-mature crude oils, conventional biomarkers become absent. However, diamondoids belonging to the class of alicyclic alkanes with cage-like interlocking molecular structures, exhibit elevated thermal stability and resist decomposition at elevated temperatures (Wei et al., 2006). Their enrichment effectively signals the maturity and extent of cracking in deep crude oil. The methyl-adamantane index (MAI) and methyl-diamantane index (MDI) were utilized for crude oil maturity determination (Chen et al., 1996):

Table 3
Values of some relevant oil thermal maturity parameters.

Well	Depth, m	MPI	Rc_1, %	MAI	MDI	Rc_2, %
TZ62	4758	1.09	1.52	0.71	0.48	1.60
TZ82	5385	1.28	1.31	0.85	0.50	1.67
TZ83	5681	1.01	1.70	0.83	0.53	1.72
TZ721	5505	1.01	1.66	/	/	/
ZG102	6060	1.33	1.57	0.81	0.48	1.61
TZ726	5535	0.62	1.86	0.84	0.47	1.58
ZG5	6460	0.78	1.68	0.77	0.58	1.85
TZ722	5750	1.16	1.10	/	/	/
TZ162	5070	1.00	1.00	0.77	0.41	1.44
ZG162-1H	6175	1.33	1.20	0.78	0.39	1.39

$$MAI = 1\text{-MA}/(1\text{-MA} + 2\text{-MA}) \quad (5)$$

$$MDI = 4\text{-MD}/(1\text{-MD} + 3\text{-MD} + 4\text{-MD}) \quad (6)$$

In Eqs. (5) and (6), 1-MA = 1-methyl-adamantane; 2-MA = 2-methyl-adamantane; 1-MD = 1-methyl-diamantane; 3-MD = 3-methyl-diamantane; 4-MD = 4-methyl-diamantane.

Among them, the relationship between MDI and Rc (equivalent vitrinite reflectance) is (Zhang and Huang, 2005):

$$Rc_2 = 2.4389 \ MDI + 0.4364 \quad (7)$$

According to Eq. (7), the MAI of this area ranges from 0.71 to 0.85 (average 0.79), and the MDI ranges from 0.39 to 0.58 (average 0.48) (Table 3). By plotting the calculated MAI and MDI values in Fig. 7(a), the maturity of different types of oil samples is mainly concentrated in the range of 1.6%–1.9%, and according to the proposed Rc calibration index, it is analyzed that the Rc_2 of crude oil is between 1.39% and 1.85%, which is a highly mature crude oil. Maturity assessments obtained through two distinct methods, aromatic and diamondoid parameters, reveal that the predominant range of crude oil maturity within the Tazhong area spans from 1.4% to 1.8% (Fig. 7(b)). Conversely, black oil maturity generally remains low, with an average value of 1.29%.

5.1.2.2. Gas maturity parameters. The stable carbon isotope composition of natural gas indicates both the organic matter type and the thermal evolution degree of the source rock. The $\delta^{13}C_1$-$C_1/(C_2+C_3)$ plate (Bernard plate) is commonly utilized to differentiate between microbial and thermogenic gases (Whiticar, 1999). Microbial gas, primarily methane, exhibits carbon isotopes enriched in ^{12}C, whereas thermogenic gas, enriched in ethane and propane, shows methane carbon isotopes enriched in ^{13}C. In this study area, all natural gas sample points fall in the region of thermogenic gas in Bernard plate (Fig. 8(a)).

The methane's carbon isotope value in natural gas increases with maturity. Following predecessors' proposed calculation formula for the equivalent maturity of coal-type gas and oil-type gas (Dai, 1992), we established an identification plate for equivalent maturity (Fig. 8(b)). The $\delta^{13}C_1$ values of condensate gas and volatile oil-associated gas in the study area are notably heavier than those of black oil associated gas, indicating higher maturity for condensate gas. Furthermore, the $\delta^{13}C_2$ values of all natural gas samples fall within the range of −40.2‰ to −30.8‰, indicative of oil-type gas in the mature to over-mature stage. The calculated maturity of condensate gas spans from 1.91% to 2.35%, with an average of 2.1%. Volatile oil-associated gas exhibits an average maturity of 1.6%, while black oil-associated gas shows the lowest maturity, averaging at 0.85%. Based on a pyrolysis simulation experiment, Prinzhofer et al. (2000) established a kerogen-cracking gas and oil-cracking gas identification plot. As shown in Fig. 8(c) and (a) modified plot

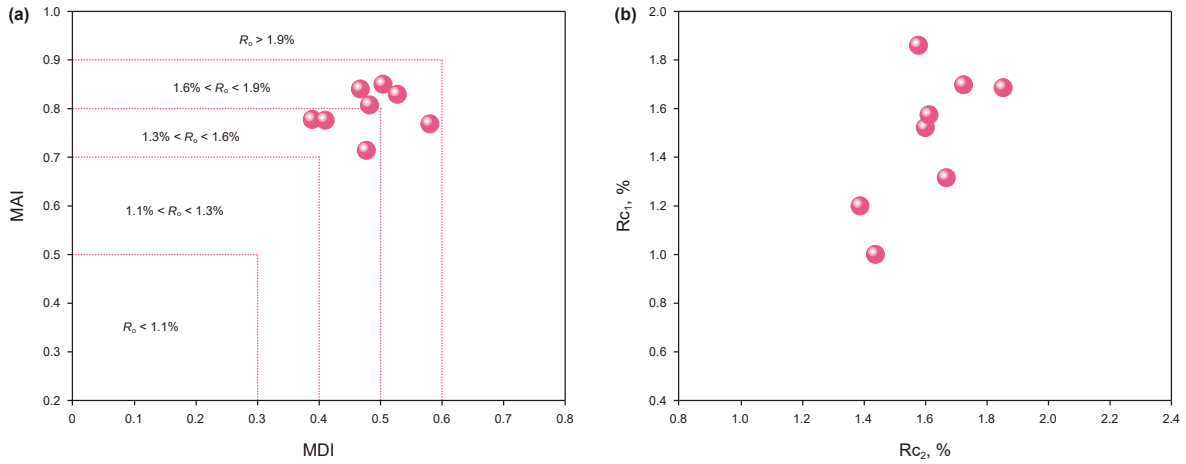

Fig. 7. Cross plots of thermal maturity parameters for the study area. Notes: **(a)** MAI (1-MA/[1-MA + 2-MA]) versus MDI (4-MD/[1-MD + 3-MD + 4-MD]); **(b)** Rc_1 versus Rc_2.

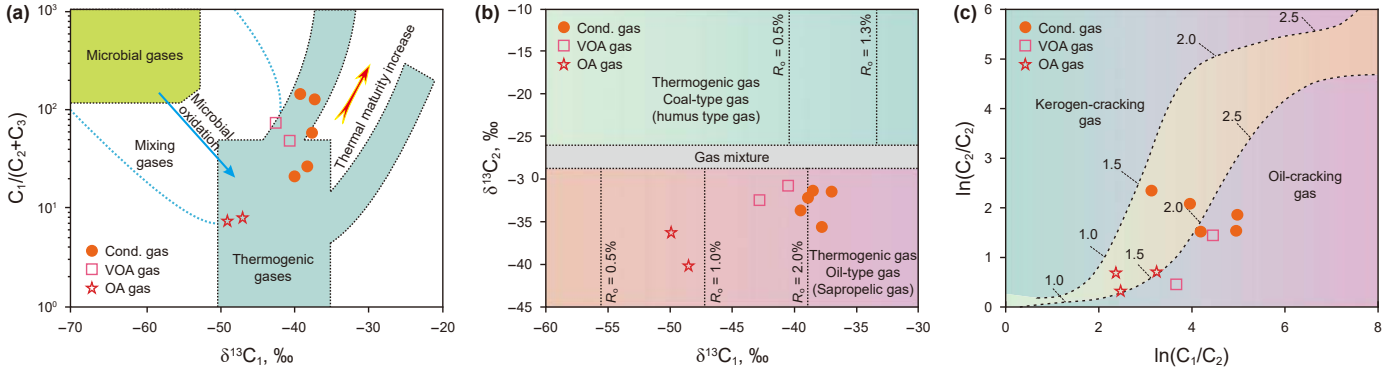

Fig. 8. Genetic type and maturity diagram of natural gases. Notes: **(a)** Diagram of $C_1/(C_2+C_3)$ ratio and the $\delta^{13}C$ values of methane (modified after Whiticar, 1999); **(b)** identification diagram of equivalent maturity of coal-type gas and oil-type gas; **(c)** discrimination plot of gas type and maturity (modified after Li et al., 2015; Zhang et al., 2022).

is used to discriminate oil type and maturity in the Tarim Basin (Li et al., 2015). Gas samples from the study site are mainly oil-cracking gas, and some samples appear in the transition zone between kerogen-cracking gas and oil-cracking gas. Consequently, the condensate gas samples in the Tazhong area are mainly typical over-mature oil-cracking dry gas, whereas the gas associated with the pool indicates the mixture of oil-cracking wet gas and some kerogen-cracking gas in the mature to high-mature stage.

It is worth noting that the maturity of condensate gas in the Tazhong area generally exceeds that of black oil, suggesting invasion of over-mature dry gas into the original pool subsequent to crude oil accumulation in the early stages. This gas invasion leads to a disparity in oil and gas maturity levels. Moreover, due to varying degrees of invasion induced by the over-mature dry gas within different structural positions of the original pool, the geochemical properties of its transformation products vary accordingly.

5.2. Quantitative assessment of multiphase in deep oil and gas

5.2.1. Indicative significance of diamondoids

Under high-intensity thermal stress, most medium to polymeric hydrocarbons in deep strata undergo substantial cracking into small molecule hydrocarbons (Wang et al., 2022). However, the distribution of *n*-alkanes in volatile oil and condensate oil within the study area exhibited a specific carbon range (Fig. 3), contrasting with primary thermogenic condensate dominated by low molecular weight hydrocarbons and containing minimal medium to polymeric hydrocarbons. This suggests that the abundant diamondoids are not products of in-situ crude oil cracking. In regions characterized by multistage charging or oil and gas mixing, when black oil is mixed with enriched diamondoids oil from other sources, it typically results in a higher concentration of diamondoids in the mixed oil compared to the original oil (Li et al., 2018; Wang et al., 2022). For instance, in this study area, the concentration of diamondoids varied significantly among different crude oil types, with condensate oil exhibiting the highest, volatile oil being the second, and black oil being the lowest (Fig. 4).

Based on the stability of diamondoids during thermal evolution, Dahl et al. (1999) proposed a method to assess the extent of crude oil cracking according to the concentration of 4-+3-methyldiamantane (4-+3-MD):

$$CR = (1 - Co/Cc) \times 100\% \quad (8)$$

In Eq. (8), CR represents the cracking rate; Co represents the content of 4-+3-MD of uncracked oil (i.e., methyldiamantanes baseline value); Cc represents the content of 4-+3-MD in cracked oil from the same source.

Currently, it is believed that the *n*-alkane baseline value of Ordovician marine phase crude oil is around 15 μg/g (Zhu et al., 2021). The concentration of 4-+3-MD in black oil samples from wells TZ162 and ZG162-1H are relatively low (21.5 μg/g and 20.7 μg/g, respectively), and close to the baseline value, with CR values of 7.0% and 3.2% respectively, indicating that they belong to

crude oil with minimal thermal cracking influence and relatively well-preserved. In contrast, the concentration of 4-+3-MD in volatile oil from well TZ726 and the condensate oil from well ZG102 is higher, at 140.2 μg/g and 169.5 μg/g respectively, with calculated CR values of 85.7% and 88.2% respectively, indicating a high degree of cracking.

The conventional understanding posits that when temperatures exceed 150 °C–160 °C and burial depths surpass 6000 m, crude oil undergoes thermal cracking, yielding natural gas (Hill et al., 2003). With the calibration of the measured borehole temperatures, we reconstructed the burial history of the wells at the study site and selected the well TZ62 for exhibition (Fig. 9). Reservoir fluid inclusion analysis is an important method to judge the accumulation period in the study of oil and gas accumulation. The homogenization temperature of fluid inclusions can effectively reconstruct the fluid filling history. The homogenization temperature of oil inclusions has very complicated controlling factors, so it is necessary to measure the homogenization temperature of saline inclusions symbiotic with oil inclusions in the same fluid inclusions combination. Two groups of petroleum-bearing inclusions were observed. The first phase is oil inclusions, and the homogenization temperature of the associated saline inclusions ranges from 90 °C to 100 °C. The second phase is mainly gas inclusions, and the homogenization temperature of the associated saline inclusions ranges from 110 °C to 120 °C. Combined with burial and thermal evolution history, the petroleum-bearing inclusions of the two periods correspond to the oil filling events of the late Hercynian period and the gas filling events of the late Himalayan period, respectively.

However, prevailing temperatures within the Ordovician pools in our study area generally remain below 140 °C, insufficient for inducing crude oil cracking. This underscores that variations in diamondoids type and concentration within crude oils are not primarily due to differing degrees of thermal cracking but rather stem from varying degrees of highly mature dry gas invasion. Rapid subsidence since the Neogene has subjected source rocks and liquid oil within the Cambrian assemblage to elevated temperature conditions. Consequently, a small fraction of residual oil reversely evaporates from a substantial volume of gas. This gas results from crude oil cracking. Initially, it was miscible with crude oil during the invasion into the original Ordovician pool. This process leads to varying degrees of diamondoid enrichment. Thus, it gives rise to the illusion of different degrees of crude oil cracking and high degrees of condensate cracking.

5.2.2. Indicative significance of sulfur compounds

Sulfur compounds of different types in crude oil exhibit significant differences in stability. Later secondary alteration processes such as mixing and TSR may increase the types and contents of sulfur compounds (Amrani, 2014; Amrani et al., 2012). Compounds like dibenzothiophenes and thiaadamantanes have good stability, and their content increases with the intensity of TSR, whereas alkylthiols and cycloalkylthiols, though generated during TSR, have poor stability (Amrani et al., 2012). Since the oil and gas supply in the Tazhong area mainly comes from Cambrian source rocks (Yang et al., 2007), the possibility of organic matter input causing differences in the abundance of sulfur compounds in crude oil is relatively low. Therefore, sulfur compounds of different types and abundances are present in the three types of crude oil. It indicates that the study area has generally undergone varying degrees of TSR influence or represents different degrees of invasion alteration by external oil and gas. The abundance of sulfur compounds is lowest in the black oil from well TZ162 (Fig. 5), similar to the original crude oil with a relatively low degree of alteration, while sulfur compounds are relatively enriched in the condensate oil and volatile oil, indicating a higher degree of TSR or invasion alteration by oil and gas.

5.2.3. Source and intensity evaluation of deep gas invasion

Since the Late Permian, continuous subsidence has been observed in the Ordovician strata of the Tazhong area (Zhu et al., 2014), reaching a maximum buried depth of 6500 m, with

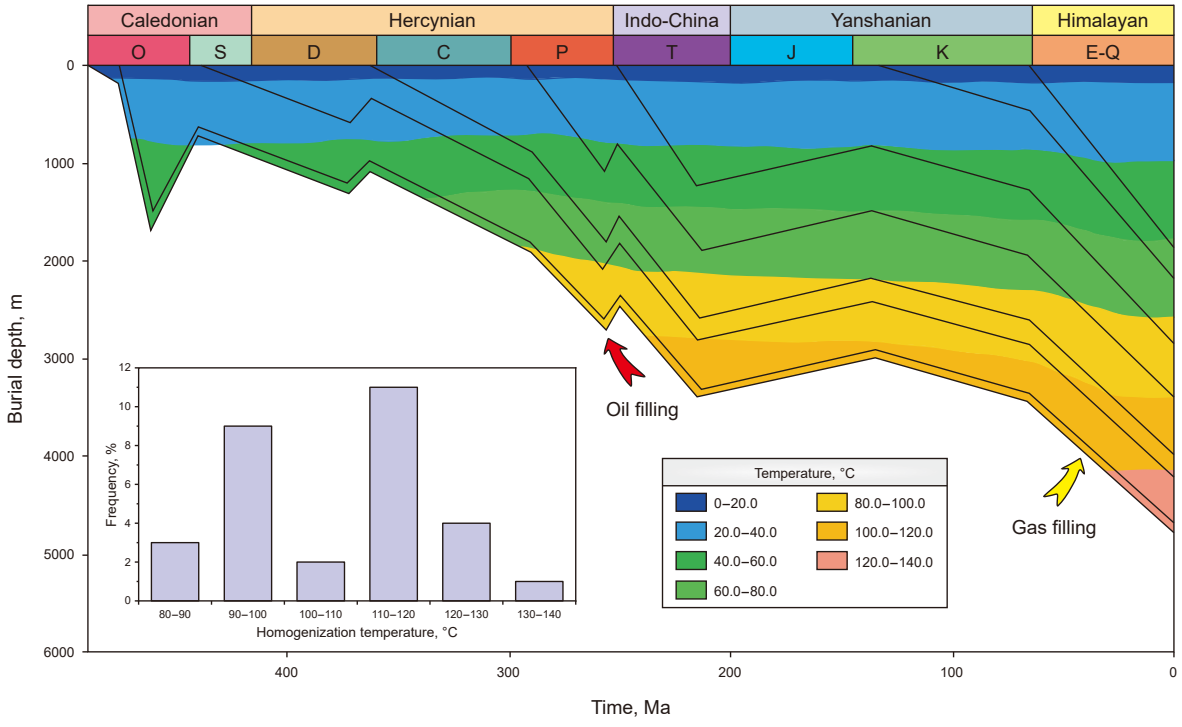

Fig. 9. Burial and thermal histories evolution of Well TZ62.

negligible presence of evaporite (Wang et al., 2024b). Consequently, the Ordovician reservoir in this region lacks the conditions conducive to in-situ crude oil cracking and TSR. In contrast, the dolomite reservoir of the Cambrian Xiaoerbulake Formation in the Tazhong area exhibits temperatures ranging between 170 °C and 240 °C, and is overlain by extensively developed evaporites (Zhu et al., 2021), serving as potential sulfur sources. Under high temperature and sulfate-rich conditions, thermal cracking and TSR induce secondary alterations in crude oil, producing dry cracked gas, condensate gas, and residual oil. Hence, the presence of diamondoids and thiadiamondoids enriched in condensate and volatile oil within the Tazhong area likely originates from the deep Cambrian strata. Continuous invasion of ultra-deep natural gas, along with its light components and secondary products from the process of crude oil cracking, into the Ordovician pool, leads to the formation of secondary condensate gas pools.

Gas invasion intensity was assessed using the exponential relationship proposed by Kissin (1987), which correlates the molar concentration logarithm of *n*-alkanes with their respective carbon numbers:

$$\ln[\mathrm{MC}(n)] = a \times n + \ln A \tag{9}$$

In Eq. (9), MC(n) represents the mass molar concentration of *n*-alkanes, while n denotes the carbon number of *n*-alkanes; a signifies the slope of the linear fitting line, and A stands for the normalization factor.

Higher gas invasion intensity exerts a greater influence on low carbon number *n*-alkanes, resulting in significant losses, while the impact on high carbon number *n*-alkanes remains minimal and adheres to the original linear relationship. Losh employed the loss of *n*-alkane (Q) to characterize gas invasion intensity quantitatively (Losh et al., 2002):

$$Q = [1 - \sum \mathrm{MnC}_i \text{ (measured value)} / \sum \mathrm{MnC}_i \text{ (unfractionated value)}] \times 100\% \tag{10}$$

In Eq. (10), $\sum \mathrm{MnC}_i$ represents the sum of the masses of *n*-alkanes with carbon numbers equal to or greater than $n\mathrm{C}_{10}$ in crude oil.

The intensity of gas invasion can be inferred from the loss of *n*-alkanes in different types of oil samples (Fig. 10): $Q \geq 80\%$ indicates a strong gas invasion in crude oil (Fig. 10(a) and (b)); $20\% \leq Q < 80\%$ suggests a weak gas invasion in crude oil (Fig. 10(c)); $0 \leq Q < 20\%$ indicates negligible gas invasion in crude oil (Fig. 10(d)).

Fig. 10(e) and (f) show the relationship between crude oil component fractionation and gas washing intensity in the study area. The index α (slope factor) indicates oil maturity, as lower index α values correspond to higher oil maturity and lighter normal alkanes. There exists a relatively strong correlation between the index α value and the 4-+3-MD parameter for the oil (Fig. 10(e)), suggesting that gas washing fractionation in the Tazhong area primarily arises from deep liquid hydrocarbon pyrolysis gas.

Index β refers to the intercept of curves related to the carbon numbers of normal alkanes and the mole concentration for the oil prior to gas washing, indicating the occurrence of gas washing and its intensity. The more the mass depletion of normal alkanes is, the greater the intercept of the curve, forming a positive correlation (Fig. 10(f)).

5.2.4. Influence of gas washing on diamondoids homologues in oil samples

Due to the varying polarities and functional groups of different diamondoids homologues present in crude oil, their distribution coefficients and solubilities differ in natural gas and crude oil (Li et al., 2018). The impact of gas washing on oil samples in the Tazhong area is a physical fractionation process, thereby altering the percentage content of diamondoids homologues in oil samples. The results of various oil samples in the Tazhong area show the percentage content of each methyl-substituted diamondoids homologues relative to the total diamondoids (Table 4), indicating a significant differential enrichment effect of gas washing on diamondoids homologues in oil samples. MAs, DMAs, and MDs are positively correlated with Q (Fig. 11(a), (b), (c)), indicating that the diamondoids with low carbon numbers are more enriched in samples with higher degrees of gas washing, occupying a higher percentage content. TMAs, TeMAs, and TMDs are negatively correlated with Q (Fig. 11(d), (e), (f)), indicating that the

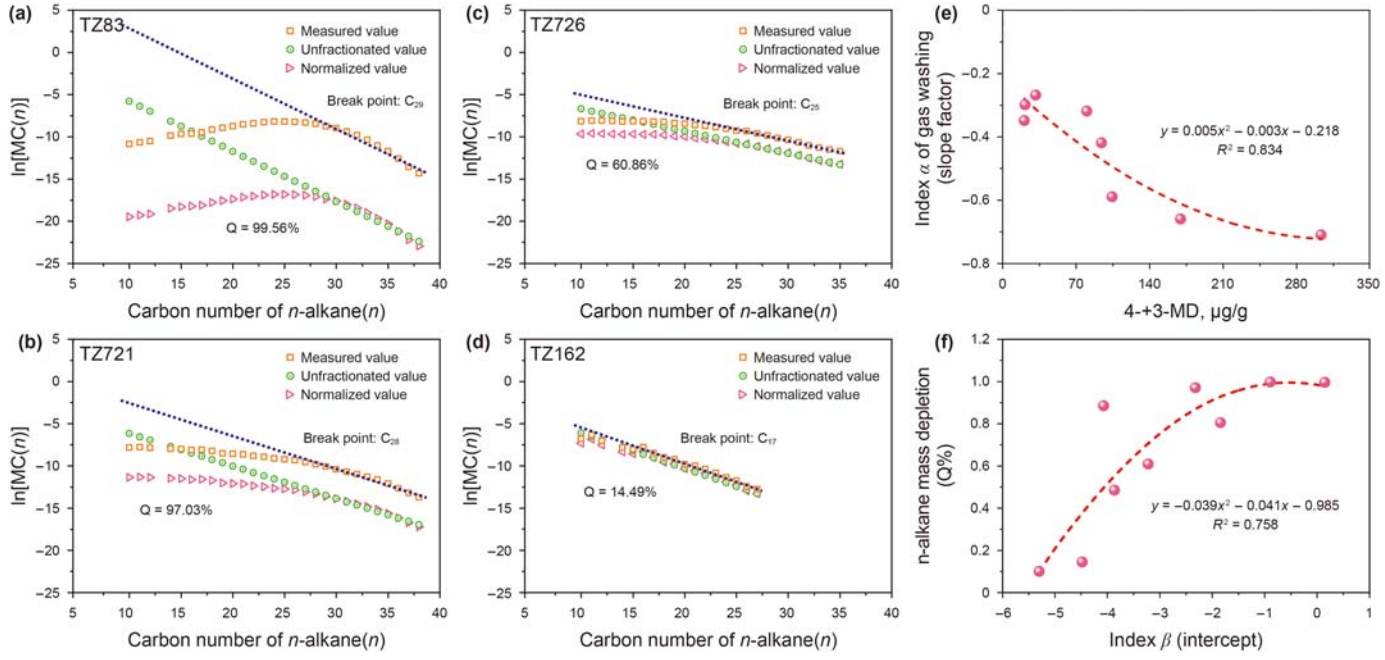

Fig. 10. Depletion of *n*-alkanes in different types of oil samples in the study area.

Table 4
Depletion of *n*-alkanes and proportion of diamondoids homologues in oil samples.

Well	Q, %	Proportion of diamondoids homologues, %									As, μg/g	Ds, μg/g	(As + Ds), μg/g
		A	MAs	DMAs	TMAs	TeMAs	D	MDs	DMDs	TMDs			
TZ62	80.49	3.83	27.13	32.81	14.60	1.30	1.32	5.09	4.57	0.53	7493.14	623.32	8116.46
TZ82	99.78	3.38	23.75	25.74	16.63	2.43	1.22	4.16	3.02	0.51	12443.38	1186.56	13629.95
TZ83	99.56	3.11	25.48	29.37	16.56	2.38	1.26	3.93	3.06	0.51	6372.80	368.17	6740.97
ZG102	88.48	3.30	22.48	26.20	17.26	2.10	1.83	4.78	3.39	0.98	5656.22	524.31	6180.53
TZ726	60.86	5.67	20.37	28.51	15.00	2.12	1.60	3.83	3.08	1.01	4608.74	398.42	5007.16
ZG5	48.65	3.03	20.09	27.31	18.62	3.35	1.48	3.85	3.73	1.09	3336.11	215.91	3552.02
TZ162	14.49	2.44	19.25	25.66	22.24	3.52	1.18	3.81	3.43	1.05	1096.64	172.83	1269.47
ZG162-1H	10.00	3.52	15.12	23.16	21.62	3.47	1.32	3.18	2.95	1.06	1527.85	181.09	1708.94

Notes: MAs: Methyladamantanes; DMAs: Dimethyladamantanes; TMAs: Trimethyladamantanes; TeMAs: Tetramethyladamantanes; MDs: Methyldiamantanes; DMDs: Dimethyldiamantanes; TMDs: Trimethyldiamantanes; As: Adamantanes; Ds: Diamantanes.

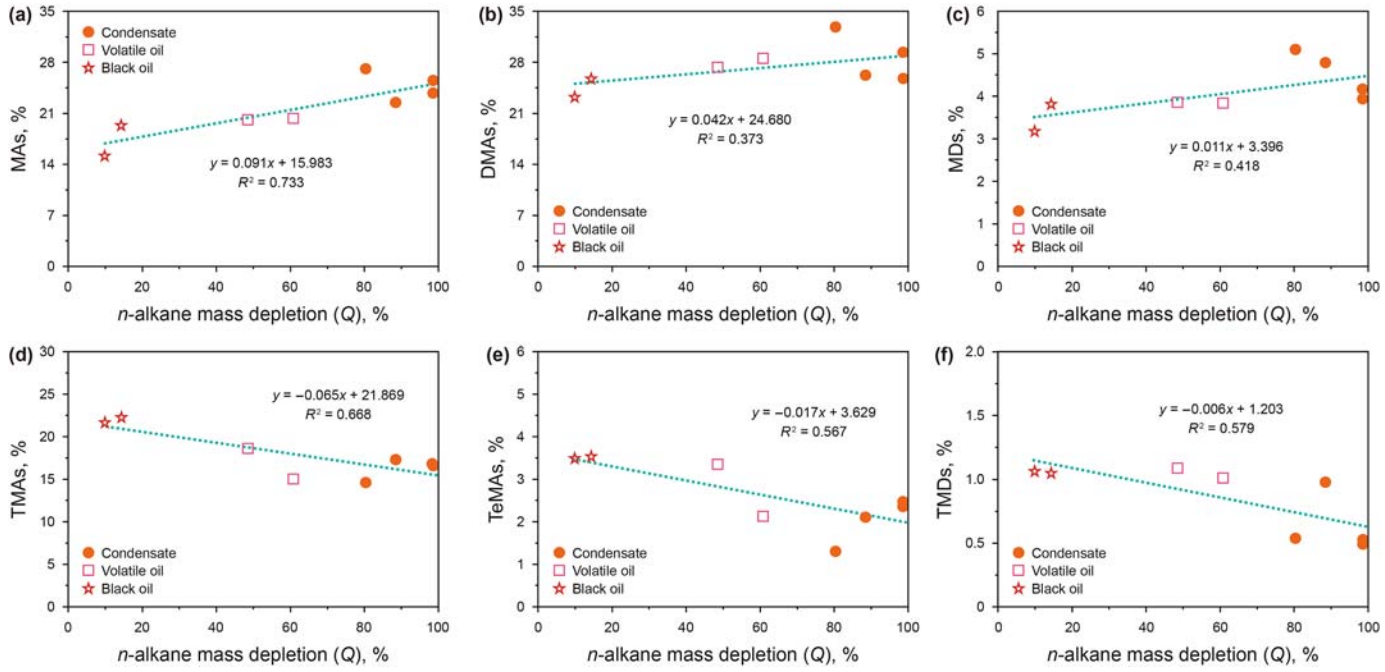

Fig. 11. Relationship between the proportion of diamondoids homologues and the depletion of *n*-alkanes.

diamondoids with high carbon numbers undergo less gas washing modification, thus leading to a relatively higher enrichment of high methyl-substituted diamondoids in oil samples with lower degrees of gas washing.

Overall, as the increase of methyl substituents among the diamondoids homologues, the saturated vapor pressure of the compounds decreased. Consequently, the percentage content of diamondoids homologues in oil samples with a lower degree of gas washing gradually became higher than those with a higher degree. Gas washing leads to a further enrichment of low carbon number diamondoids in crude oil, to some extent, enhancing the total content of adamantanes in crude oil. For instance, in the high gas washing degree sample from well TZ83, the total content of adamantanes accounts for about 95% of the total content of diamondoids, while in the low gas washing degree sample from well TZ162, the proportion is approximately 86%. However, during this physical enrichment process of gas washing, no new diamondoids are generated. Therefore, the diamondoids enriched in crude oil due to gas washing modification are mainly adamantanes, and the increase of total diamondoids content is limited. Quantitative evaluation of gas invasion intensity can be conducted based on variations in the contents of adamantanes (As) and diamantanes (Ds) in oil samples subjected to different degrees of gas washing alteration. Gas invasion intensity can be classified into strong gas invasion (As $\geq$ 5000 μg/g, Ds $\geq$ 400 μg/g), weak gas invasion (3000 μg/g $\leq$ As $<$ 5000 μg/g, 200 μg/g $\leq$ Ds $<$ 400 μg/g), and negligible gas invasion (As $<$ 3000 μg/g, Ds $<$ 200 μg/g).

5.3. The dynamic evolution of deep petroleum phase

The condensate gas pools in Tazhong Uplift are primarily secondary condensate gas pool formed by the late-stage gas invasion altering the early paleo-oil pools. The phase fractionation induced by the charging of external dry gas along the Tazhong 1 thrust fault belt into the Ordovician paleo-oil pools causes fractionation losses of light to medium components from the crude oil (Zhang et al., 2019), leading to secondary changes in hydrocarbon properties and phases. The evolution model of multistage hydrocarbon charging and multiphase pools in the Tazhong area is illustrated in Fig. 12:

The formation stage of Cambrian paleo-oil pools (Fig. 12(a)): Regional exposure events and fault activities improved the Ordovician reef-shoal limestone reservoirs, and the fracture system developed, forming high-quality fracture-cavity reservoirs. The high-quality source rocks of Lower Cambrian entered the oil generation stage, forming a series of paleo-oil pools within the

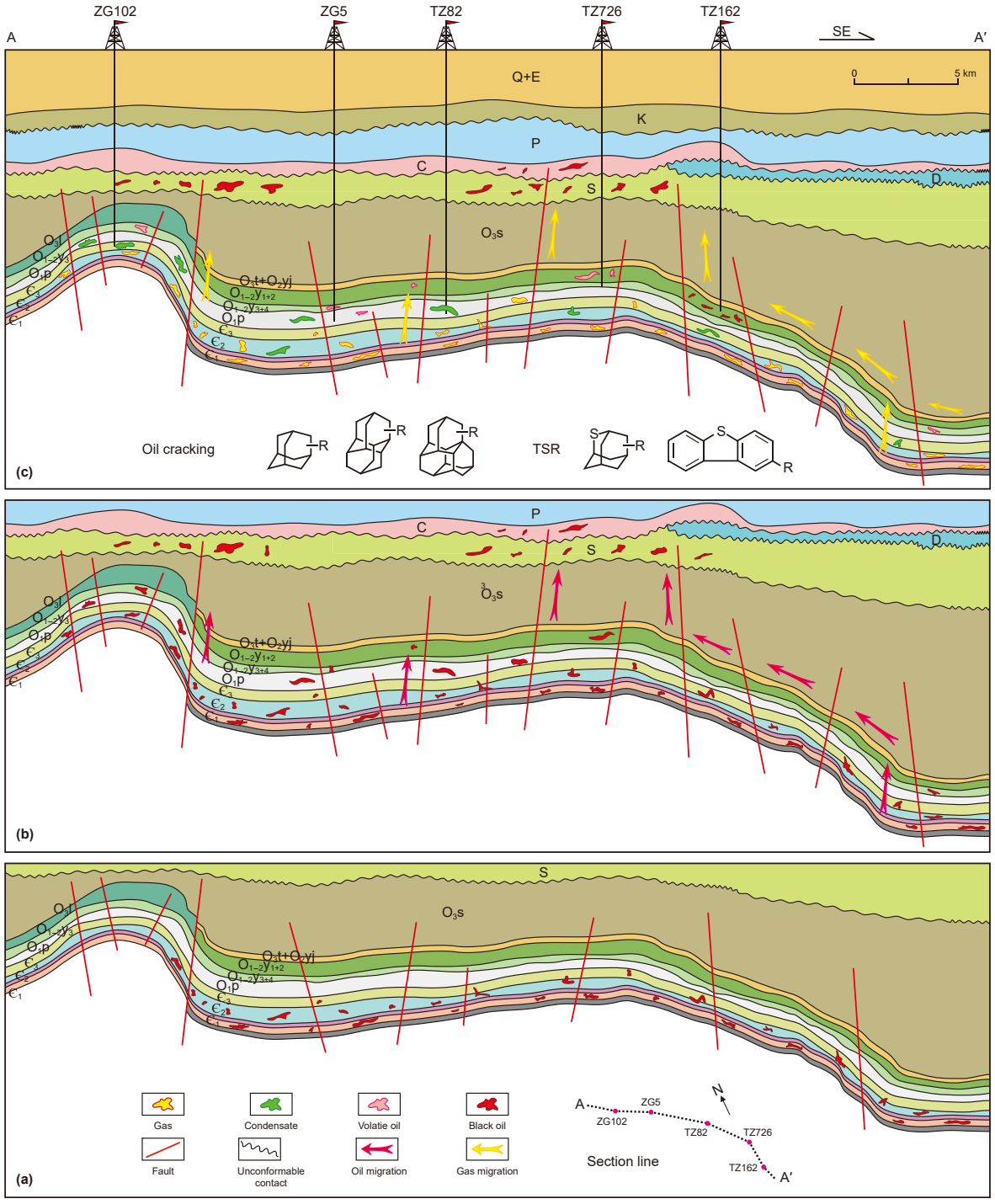

Fig. 12. Evolution model of multistage hydrocarbon charging and multiphase pools in the Tazhong area.

Cambrian reservoir combination.

The formation stage of Ordovician pools and Cambrian gas source (Fig. 12(b)): Late Silurian strike-slip faults developed in the Tazhong area, controlling the basic structural pattern. The deep major faults connected with the Cambrian source rocks. Oil and gas migrated vertically along the fault system into the Ordovician reservoirs, forming extensive distributions of black oil pools (with low gas-oil ratio and moderate maturity). Additionally, part of the crude oil migrated into the Silurian and Carboniferous-Permian strata.

The formation stage of gas invasion and alteration (Fig. 12(c)): After the Late Permian hydrocarbon accumulation, the area entered a stable subsidence stage, with moderate temperature conditions in the Ordovician pools (around 120 °C), ensuring good preservation. Since the Neogene, the basin has entered a rapid subsidence stage, and the thickness of overlying strata has increased by more than 2000 m (Zhu et al., 2023). Under the influence of thermal cracking and TSR at high temperature (>200 °C), the Cambrian paleo-oil pools have been gradually transformed into dry gas and condensed gas, and enriched with diamondoids and sulfur compounds. The intracontinental orogeny triggered local adjustments

of the fault system in the Tazhong area. This caused a large amount of TSR-altered cracking gas to be charged into the primary Ordovician pools, leading to an increase in the gas-oil ratio of the oil and gas pools, associating gas turning dry, and secondary compounds gradually enriching in the crude oil. Developed faults often form migration pathways with good permeability, so the closer to the gas source fault, the higher the degree of gas invasion. Strong gas invasion gradually transforms black oil pools into volatile oil pools. As the gas-oil ratio significantly increases until it exceeds the critical point of oil phase retention under reservoir temperature and pressure conditions, the liquid phase condenses into the gas phase, forming secondary condensate gas pools.

6. Conclusion

The Ordovician condensate oil in the Tazhong area is characterized by high wax content and density compared to black oil. The condensate gas is predominantly dry gas with heavier carbon isotopes, indicating highly mature oil-cracking gas. However, the Ordovician pools have not reached the temperature threshold for crude oil cracking, suggesting that the cracking gas originates from Cambrian paleo-oil pools. The high density, high wax crude oil is primarily due to natural gas fractionation.

GC × GC-TOFMS analysis revealed abundant diamondoids and sulfur compounds in the Ordovician condensate oil, a result of intense cracking of Cambrian paleo-oil pools. These secondary compounds, likely dissolved in cracking gas under high-pressure and high-temperature conditions, migrate along deep faults and accumulate in shallow layers, contributing to the complex oil and gas pools.

The formation of condensate gas pools in the Tazhong Uplift is linked to deep faults connecting Cambrian subsalt hydrocarbon resources. The area shows significant potential, with large-scale condensate and dry gas pools formed by thermal cracking and TSR modification. As drilling technologies improve and geological understanding advances, this region holds considerable exploration promise. Optimizing well locations and drilling strategies, based on a thorough understanding of fault systems, will be key for future exploration.

CRediT authorship contribution statement

Jia-Kai Hou: Writing – review & editing, Writing – original draft, Formal analysis. **Zhi-Yao Zhang:** Writing – review & editing, Software, Resources, Conceptualization. **Guang-You Zhu:** Resources, Methodology, Investigation. **Jian-Fa Han:** Software, Resources, Conceptualization. **Lin-Xian Chi:** Resources. **Zi-Guang Zhu:** Formal analysis, Data curation. **Hong-Bin Li:** Software, Resources. **Meng-Qi Li:** Methodology, Formal analysis. **Rui-Lin Wang:** Software.

Declaration of competing interest

The authors declare that they have no known competing financial interests or personal relationships that could have appeared to influence the work reported in this paper.

Acknowledgement

This study was jointly supported by the National Natural Science Foundation of China (Grant Nos. 42002178 and 42472203), "CUG Scholar" Scientific Research Funds at China University of Geosciences (Grant No. 2022193), and China National Petroleum Corporation (CNPC) Scientific Research and Technology Development Projects (Grant Nos. 2019B-04 and 2021DJ05). We acknowledge Tarim Oilfield Company, PetroChina, for data contribution and sample collection. We thank Dr. Sheng-Bao Shi at China University of Petroleum (Beijing) for assistance with GC and GC × GC-TOFMS analysis.

References

Amrani, A., 2014. Organosulfur compounds: molecular and isotopic evolution from biota to oil and gas. Annu. Rev. Earth Planet Sci. 42, 733–768. https://doi.org/10.1146/annurev-earth-050212-124126.

Amrani, A., Deev, A., Sessions, A., Tang, Y.C., Adkins, J., Hill, R., Moldowan, J., Wei, Z.B., 2012. The sulfur-isotopic compositions of benzothiophenes and dibenzothiophenes as a proxy for thermochemical sulfate reduction. Geochem. Cosmochim. Acta 84, 152–164. https://doi.org/10.1016/j.gca.2012.01.023.

Azevedo, D.A., Tamanqueira, J.B., Dias, J.C.M., Carmo, A.P.B., Landau, L., Gonçalves, F.T.T., 2008. Multivariate statistical analysis of diamondoid and biomarker data from Brazilian basin oil samples. Fuel 87, 2122–2130. https://doi.org/10.1016/j.fuel.2007.11.005.

Bian, J.J., Hou, D.J., Cui, Y.W., Zhu, X.X., 2023. Geochemical characteristics and origin of the ultra-deep hydrocarbons from the Shunbei Oilfield in the Tarim Basin, China: insight from molecular biomarkers and carbon isotope geochemistry. Mar. Petrol. Geol. 158, 106542. https://doi.org/10.1016/j.marpetgeo.2023.106542.

Chen, J.H., Fu, J.M., Sheng, G.Y., Liu, D.H., Zhang, J.J., 1996. Diamondoid hydrocarbon ratios: novel maturity indices for highly mature crude oils. Org. Geochem. 25 (3), 179–190. https://doi.org/10.1016/S0146-6380(96)00125-8.

Dahl, J.E., Moldowan, J.M., Peters, K.E., Claypool, G.E., Rooney, M.A., Michael, G.E., Mello, M.R., Kohnen, M.L., 1999. Diamondoid hydrocarbons as indicators of natural oil cracking. Nature 399, 54–57. https://doi.org/10.1038/19953.

Dahl, J.E.P., Liu, S.G., Robert, M.K. Carlson, 2002. Isolation and structure of higher diamondoids, nanometer-sized diamond molecules. Science. 299, 96–99. https://doi.org/10.1126/science.1078239.

Dai, J.X., Zou, C.N., Dong, D.Z., Ni, Y.Y., Wu, W., Gong, D.Y., Wang, Y.M., Huang, S.P., Huang, J.L., Fang, C.C., Liu, D., 2016. Geochemical characteristics of marine and terrestrial shale gas in China. Mar. Petrol. Geol. 76, 444–463. https://doi.org/10.1016/j.marpetgeo.2016.04.027.

Dai, J.X., 1992. Identification of various alkane gases. Sci. China (2), 185–193. https://doi.org/10.1360/zb1992-22-2-185.

Danesh, A., 1998. PVT and phase behaviour of petroleum reservoir fluids. Energy Power 47, 1061–1082. https://doi.org/10.1016/s0376-7361(98)80028-9.

Dyman, T.S., Crovelli, R.A., Bartberger, C.E., Takahashi, K.I., 2002. Worldwide estimates of deep natural gas resources based on the U.S. Geological survey world petroleum assessment 2000. Nat. Resour. Res. 11 (3), 207–218. https://doi.org/10.4043/13036-ms.

Guo, X.S., Hu, Z.Q., Li, S.J., Zheng, L.J., Zhu, D.Y., Liu, J.L., Shen, B.J., Du, W., Yu, L.J., Liu, Z.Q., 2023. Progress and prospect of natural gas exploration and research in deep and ultra-deep strata. Petroleum Sci. Bull. 8 (4), 461–474. https://doi.org/10.3969/j.issn.2096-1693.2023.04.035.

Gvirtzman, Z., Ward, S.A., Geoffrey, S.E., Ronald, J.H., Michael, J.M., Wei, Z.B., Amrani, A., 2015. Compound-specific sulfur isotope analysis of thiadiamondoids of oils from the Smackover Formation, USA. Geochem. Cosmochim. Acta 167, 144–161. https://doi.org/10.1016/j.gca.2015.07.008.

Han, J.F., Mei, L.F., Yang, H.J., Wu, G.H., Xu, Z.M., Zhu, G.Y., 2007. Study on hydrocarbon source and migration and accumulation of Ordovician carbonate reef-beach complex in Tazhong area, Tarim Basin. Nat. Gas Geosci. (3), 426–435. https://doi.org/10.3969/j.issn.1672-1926.2007.03.023.

Han, J.F., Wu, G.H., Yang, H.J., Dai, L., Su, Z., Tang, H., Xiong, C., 2021. Type and genesis of condensate gas reservoir in the Tazhong uplift of the Tarim Basin. Nat. Gas. Ind. 41 (7), 24–32. https://doi.org/10.3787/j.issn.1000-0976.2021.07.003.

Han, J.F., Zhang, H.Z., Yu, H.F., Ji, Y.G., Sun, C.H., Han, J., Dong, R.X., 2012. Hydrocarbon accumulation characteristic and exploration on large marine carbonate condensate field in Tazhong Uplift. Acta petrologica 28 (3), 769–782. https://doi.org/10.1177/014459879401200112.

Hill, R.J., Tang, Y.C., Isaac, R.K., 2003. Insights into oil cracking based on laboratory experiments. Org. Geochem. 34, 1651–1672. https://doi.org/10.1016/S0146-6380(03)00173-6.

Huang, H.P., Zhang, S.C., Su, J., 2016. Palaeozoic oil–source correlation in the Tarim Basin, NW China: a review. Org. Geochem. 94, 32–46. https://doi.org/10.1016/j.orggeochem.2016.01.008.

Jia, C.Z., Zhang, S.C., 2023. The formation of marine ultra-deep petroleum in China. Acta Geol. Sin. 97 (9), 2775–2801. https://doi.org/10.19762/j.cnki.dizhixuebao.2023201.

Jin, Z.J., Cai, L.G., 2007. Inheritance and innovation of marine petroleum geological theory in China. Acta Geol. Sin. (8), 1017–1024. https://doi.org/10.3321/j.issn:0001-5717.2007.08.001.

Kissin, Y.V., 1987. Catagenesis and composition of petroleum: origin of n-alkanes and isoalkanes in petroleum crudes. Geochem. Cosmochim. Acta 51 (9), 2445–2457. https://doi.org/10.1016/0016-7037(87)90296-1.

Kontogeorgis, G., Ioannis, E., 2010. Equations of state: From the ideas of van der Waals to association theories. J. Supercrit. Fluids 55, 421–437. https://doi.org/10.1016/j.supflu.2010.10.023.

Li, C.X., Jia, C.Z., Li, B.L., Yang, G., Yang, H.J., Luo, C.S., Han, J.F., Wang, X.F., 2009. Paleozoic fault distribution and tectonic evolution on the north slope of

Tazhong Low uplift in Tarim Basin. Acta Geol. Sin. 83 (8), 1065–1073. https://doi.org/10.3321/j.issn:0001-5717.2009.08.002.
Li, Y., Xue, Z.J., Cheng, Z., Jiang, H.J., Wang, R.Y., 2020a. Progress and development directions of deep oil and gas exploration and development in China. China Petrol. Expl. 25 (1), 45–57. https://doi.org/10.3969/j.issn.1672-7703.2020.01.005.
Li, J.F., Zhang, Z.Y., Zhu, G.Y., Li, T.T., Zhao, K., Chi, L.X., Yan, H.H., 2020b. The origin and accumulation of ultra-deep oil in Halahatang area, northern Tarim Basin. J. Petrol. Sci. Eng. 195, 107898. https://doi.org/10.1016/j.petrol.2020.107898.
Li, J., Xie, Z., Wei, G., Li, Z., Wang, W., 2015. Geochemical characteristics and exploration potential of natural gas in Anyue gas field, the largest uncompartmentalized carbonate gas field in China. In: The 15th National Meeting on Organic Geochemistry in China, Qingdao. https://doi.org/10.1260/0144-5987.33.6.827.
Li, Y., Xiong, Y.Q., Liang, Q.Y., Fang, C.C., Chen, Y., Wang, X.T., Liao, Z.W., Peng, P.A., 2018. The application of diamondoid indices in the Tarim oils. AAPG (Am. Assoc. Pet. Geol.) Bull. 102 (2), 267–291. https://doi.org/10.1306/0424171518217073.
Li, S.M., Pang, X.Q., Jin, Z.J., Yang, H.J., Xiao, Z.Y., Gu, Q.Y., Zhang, B.S., 2010. Petroleum source in the Tazhong Uplift, Tarim Basin: new insights from geochemical and fluid inclusion data. Org. Geochem. 41 (6), 531–553. https://doi.org/10.1016/j.orggeochem.2010.02.018.
Li, F., Zhu, G.Y., Lv, X.X., Zhang, Z.Y., Wu, Z.H., Xue, N., He, T., Wang, R., 2021. Source dispute of Paleozoic Marine hydrocarbon and identification of main Cambrian source rocks in Tarim Basin. Acta Pet. Sin. 42 (11), 1417–1436. https://doi.org/10.7623/syxb202111002.
Losh, S., Lawrence, C., Peter, M., 2002. Gas washing of oil along a regional transect, offshore Louisiana. Org. Geochem. 33 (6), 655–663. https://doi.org/10.1016/S0146-6380(02)00025-6.
Lu, Z.D., Ping, H.W., Chen, H.H., Zhang, Y.Q., Xie, Z., Zhang, Y.T., Chen, Z.L., Yang, X., Zhang, X.L., Yang, K., Li, X.Q., 2024. Geochemical characteristics of Ordovician crude oils in the FI17 strike-slip fault zone of the Fuman oilfield, Tarim basin: implications for ultra-deep hydrocarbon accumulation in the Tarim basin. Mar. Petrol. Geol. 163, 106800. https://doi.org/10.1016/j.marpetgeo.2024.106800.
Luo, M.X., Cao, Z.C., Xu, Q.Q., Liu, Y.L., Shang, K., 2024. Geochemical characteristics and geological significance of sinian crude oil from well tashen 5, tahe oilfield, Tarim Basin. Bull. Geol. Sci. Tech. 43 (1), 135–149. https://doi.org/10.19509/j.cnki.dzkq.tb20230194.
Lv, X.X., Jiao, W.W., Zhou, X.Y., Li, J.J., Yu, H.F., Ning, Y., 2009. Paleozoic carbonate hydrocarbon accumulation zones in Tazhong uplift, Tarim Basin, western China. Energy Explor. Exploit. 27, 69–90. https://doi.org/10.1016/S0920-4105(03)00147-5.
Masterson, W.D., Leon, I.P.D., Albert, G.H., Ann, L.F., Leroy, E., 2001. Evidence for biodegradation and evaporative fractionation in west sak, kuparuk and prudhoe bay field areas, North Slope, Alaska. Org. Geochem. 32 (3), 411–441. https://doi.org/10.1016/S0146-6380(00)00187-X.
Maxwell, J.C., 2011. Van der Waals on the Continuity of the Gaseous and Liquid States. In: Maxwell, J.C., Niven, W.D. (Eds.), The Scientific Papers of James Clerk Maxwell. Cambridge University Press, Cambridge, pp. 407–415. https://doi.org/10.1017/cbo9780511710377.044.
Pang, H., Chen, J.Q., Pang, X.Q., Liu, K.Y., Liu, L.F., Xiang, C.F., Li, S.M., 2013. Analysis of secondary migration of hydrocarbons in the Ordovician carbonate reservoirs in the Tazhong uplift, Tarim Basin, China. AAPG (Am. Assoc. Pet. Geol.) Bull. 97 (10), 1765–1783. https://doi.org/10.1306/04231312099.
Prinzhofer, A., Mello, M., Takaki, T., 2000. Geochemical characterization of natural gas: a physical multivariable approach and its applications in maturity and migration estimates. Am. Assoc. Petrol. Geol. Bull. 84, 1152–1172. https://doi.org/10.1306/8626d35b-173b-11d7-8645000102c1865d.
Radke, M., 1983. The Methylphenanthrene Index (MPI) : a maturity parameter based on aromatic hydrocarbons. Sci. Res. (N. Y.) 4 (4), 504–512. https://doi.org/10.1016/3251.2005.01.014.
Thompson, K.F.M., 1983. Classification and thermal history of petroleum based on light hydrocarbons. Geochem. Cosmochim. Acta 47 (2), 303–316. https://doi.org/10.1016/0016-7037(83)90143-6.
Thompson, K.F.M., 1987. Fractionated aromatic petroleums and the generation of gas-condensates. Org. Geochem. 11 (6), 573–590. https://doi.org/10.1016/0146-6380(87)90011-8.
Wang, H.T., Zhang, S.C., Weng, N., Li, W., Qin, S.F., Ma, W.L., 2012. Analysis of condensate oil by comprehensive two-dimensional gas chromatography. Petrol. Explor. Dev. 39 (1), 132–138. https://doi.org/10.1016/S1876-3804(12)60025-1.
Wang, R.L., Wang, T., Zhu, G.Y., Wang, M., Zhang, Z.Y., Wen, Z.G., 2022. Abundance difference and influence mechanism of different diamondoid isomers in crude oil:Taking Lungu area of Tarim Basin as an example. Nat. Gas Geosci. 33 (12), 2087–2099. https://doi.org/10.11764/j.issn.1672-1926.2022.07.012.
Wang, W.Y., Pang, X.Q., Wang, Y.P., Chen, Z.X., Jiang, F.J., Chen, Y., 2024a. Quantitative prediction model for the depth limit of oil accumulation in the deep carbonate rocks: a case study of Lower Ordovician in Tazhong area of Tarim Basin. Pet. Sci. 21 (1), 115–124. https://doi.org/10.1016/j.petsci.2023.11.013.
Wang, W.Y., Pang, X.Q., Wang, Y.P., Jiang, F.J., Chen, Y., Chen, Z.X., 2024b. Critical condition of the depth limit of oil accumulation of carbonate reservoirs and its exploration significance in the lower ordovician of the Tazhong area in the Tarim Basin. ACS Omega 9 (1), 1443–1453. https://doi.org/10.1021/acsomega.3c07793.
Wei, Z.B., Michael, M.J., Adina, P., 2006. Diamondoids and molecular biomarkers generated from modern sediments in the absence and presence of minerals during hydrous pyrolysis. Org. Geochem. 37 (8), 891–911. https://doi.org/10.1016/j.orggeochem.2006.04.008.
Whiticar, M.J., 1999. Carbon and hydrogen isotope systematics of bacterial formation and oxidation of methane. Chem. Geol. 161 (1), 291–314. https://doi.org/10.1016/S0009-2541(99)00092-3.
Yang, H.J., Han, J.F., Chen, L.X., Wu, G.H., Ji, Y.G., 2007. Characteristics and patterns of complex hydrocarbon accumulation in the Lower Paleozoic carbonate rocks of the Tazhong Palaeouplift. Oil Gas Geol. (6), 784–790. https://doi.org/10.1016/ojs.2007.103888.
Yang, H.J., Zhu, G.Y., Han, J.F., Wu, F.F., Ji, Y.G., Su, J., Zhang, H.Z., Wang, Y., 2011. Conditions and mechanism of hydrocarbon accumulation in large reef-bank karst oil/gasfields of Tazhong area,Tarim basin. Acta petrologica 27 (6), 1865–1885. https://doi.org/10.11764/j.issn.1672-1926.2009.05.695.
Zhang, H., Cai, Z.X., Hao, F., Qi, L.X., Yun, L., Jiang, L., 2018a. Hydrogeomorphologic architecture of epikarst reservoirs in the middle-lower ordovician, Tazhong uplift, Tarim Basin, China. Mar. Petrol. Geol. 98, 146–161. https://doi.org/10.1016/j.marpetgeo.2018.08.008.
Zhang, N., Wang, Z.M., Yang, H.J., Xing, Y.L., Zhao, R.H., 2010. The stages and significance of ordovician fluid inclusions in Tazhong No.1 slope break. Xinjing Pet. Geol. 31 (1), 22–25. https://doi.org/10.1190/ice2015-2211490.
Zhang, S.C., Gao, Z.Y., Li, J.J., Zhang, B.M., Gu, Q.Y., Lu, Y.H., 2012. Identification and distribution of marine hydrocarbon source rocks in the Ordovician and Cambrian of the Tarim Basin. Petrol. Explor. Dev. 39, 305–314. https://doi.org/10.1016/S1876-3804(12)60046-9.
Zhang, S.C., Huang, H.P., Su, J., Liu, M., Wang, X.M., Hu, J., 2015. Geochemistry of Paleozoic marine petroleum from the Tarim Basin, NW China: Part 5. Effect of maturation, TSR and mixing on the occurrence and distribution of alkyldibenzothiophenes. Org. Geochem. 86, 5–18. https://doi.org/10.1016/j.orggeochem.2015.05.008.
Zhang, S.C., Huang, H.P., 2005. Geochemistry of palaeozoic marine petroleum from the Tarim Basin, NW China. Part 2: maturity assessment. Org. Geochem. 36 (8), 1215–1225. https://doi.org/10.1016/j.orggeochem.2005.01.014.
Zhang, Z.Y., Zhang, Y.J., Zhu, G.Y., Han, J.F., Chi, L.X., 2024a. Multiphase pools caused by gas invasion in deep Ordovician carbonates from the Tazhong area, Tarim Basin, China. AAPG (Am. Assoc. Pet. Geol.) Bull. 108 (5), 817–848. https://doi.org/10.1306/12212318282.
Zhang, Z.Y., Wang, H., Zhu, G.Y., Sun, C.H., Ge, X., Chi, L.X., Li, J.F., 2022. Phase fractionation and oil mixing as contributors to complex petroleum phase in deep strata: a case study from LG7 block in the Tarim Basin, China. Mar. Petrol. Geol. 140, 105660. https://doi.org/10.1016/j.marpetgeo.2022.105660.
Zhang, Z.Y., Zhang, Y.J., Zhu, G.Y., Chi, L.X., Han, J.F., 2019. Impacts of thermochemical sulfate reduction, oil cracking, and gas mixing on the petroleum fluid phase in the Tazhong area, Tarim Basin, China. Energy Fuels 33, 968–978. https://doi.org/10.1021/acs.energyfuels.8b03931.s001.
Zhang, Z.Y., Zhu, G.Y., Chen, W.Y., Wu, L., Ren, R., Zhang, C.L., 2024b. Cryogenian–Cambrian tectono-sedimentary evolution, paleoclimate and environment effects, and formation of petroleum resources in the Tarim Block. Earth Sci. Rev. 248, 104632. https://doi.org/10.1016/j.earscirev.2023.104632.
Zhang, Z.Y., Zhu, G.Y., Zhang, Y.J., Han, J.F., Li, T.T., Wang, E.Z., Greenwood, P., 2018b. The origin and accumulation of multi-phase reservoirs in the east Tabei uplift, Tarim Basin, China. Mar. Petrol. Geol. 98, 533–553. https://doi.org/10.1016/j.marpetgeo.2018.08.036.
Zhu, G.Y., Chen, F.R., Wang, M., Zhang, Z.Y., Ren, R., Wu, L., 2018. Discovery of the lower Cambrian high-quality source rocks and deep oil and gas exploration potential in the Tarim Basin, China. AAPG (Am. Assoc. Pet. Geol.) Bull. 102 (10), 2123–2151. https://doi.org/10.1306/03141817183.
Zhu, G.Y., Zhang, B.T., Yang, H.J., Su, J., Liu, K.Y., Zhu, Y.F., 2014. Secondary alteration to ancient oil reservoirs by late gas filling in the Tazhong area, Tarim Basin. J. Petrol. Sci. Eng. 122, 240–256. https://doi.org/10.1016/j.petrol.2014.07.017.
Zhu, G.Y., Zhang, Z.Y., Jiang, H., Yan, L., Chen, W.Y., Li, T.T., Li, X., 2023. Evolution of the Cryogenian cratonic basins in China, paleo-oceanic environment and hydrocarbon generation mechanism of ancient source rocks, and exploration potential in 10,000 m-deep strata. Earth Sci. Rev. 244, 104506. https://doi.org/10.1016/j.earscirev.2023.104506.
Zhu, G.Y., Zhang, Z.Y., Alexei, V.M., Zhou, X.X., Yang, H.J., Han, J.F., 2019. Diamondoids as tracers of late gas charge in oil reservoirs: example from the Tazhong area, Tarim Basin, China. Fuel 253, 998–1017. https://doi.org/10.1016/j.fuel.2019.05.030.
Zhu, G.Y., Li, J.F., Zhang, Z.Y., 2021. Origin of deep petroleum phase state diversity and evaluation of secondary geochemical intensity—a case study of marine oil and gas in Tarim Basin. Earth Sci. 1–17. https://doi.org/10.1016/s1876-3804(25)60536-2.